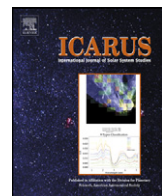




Contents lists available at ScienceDirect

Icarus

www.elsevier.com/locate/icarus

Searching for high alumina mare basalts using Clementine UVVIS and Lunar Prospector GRS data: Mare Fecunditatis and Mare Imbrium

Georgiana Y. Kramer ^{a,b,*}, Bradley L. Jolliff ^c, Clive R. Neal ^b^a Bear Fight Center, 22 Fiddler's Rd, Winthrop, WA 98862, USA^b Department of Civil Engineering and Geological Sciences, University of Notre Dame, IN 46556, USA^c Department of Earth and Planetary Sciences, Washington University, St. Louis, MO 63130, USA

ARTICLE INFO

Article history:

Received 19 February 2008

Revised 24 May 2008

Available online 4 July 2008

Keywords:

Moon, surface

ABSTRACT

In the context of sample evidence alone, the high-alumina (HA) basalts appear to be an unique, and rare variety of mare basalt. In addition to their distinct chemistry, radiometric dating reveals these basalts to be among the oldest sampled mare basalts. Yet, HA basalts were sampled by four missions spanning a lateral range of ~2400 km, with ages demonstrating that aluminous volcanism lasted at least 1 billion years. This evidence suggests that HA basalts may be a widespread phenomenon on the Moon. Knowing the distribution of HA mare basalts on the lunar surface has significance for models of the origin and the evolution of the Lunar Magma Ocean. Surface exposures of HA basalts can be detected with compositional remote sensing data from Lunar Prospector Gamma Ray Spectrometer and Clementine. We searched the lunar surface for regions of interest (ROIs) that correspond to the intersection of three compositional constraints taken from values of sampled HA basalts: 12–18 wt% FeO, 1.5–5 wt% TiO₂, and 0–4 ppm Th. We then determined the “true” (unobscured by regolith) composition of basalt units by analyzing the rims and proximal ejecta of small impacts (0.4–4 km in diameter) into the mare surface of these ROIs. This paper focuses on two ROIs that are the best candidates for sources of sampled HA basalts: Mare Fecunditatis, the landing site of Luna 16; and northern Mare Imbrium, hypothesized origin of the Apollo 14 HA basalts. We demonstrate our technique's ability for delineating discrete basalt units and determining which is the best compositional match to the HA basalts sampled by each mission. We identified two units in Mare Fecunditatis that spectrally resemble HA basalts, although only one unit (IIltm) is consistent with the compositional and relative age of the Luna 16 HA samples. Northern Mare Imbrium also reveals two units that are within the compositional constraints of HA basalts, with one (IIltm) best matching the composition of the basalts sampled by Apollo 14.

© 2008 Elsevier Inc. All rights reserved.

1. Introduction

The Soviet Luna 16 and American Apollo 14 sample return missions brought to Earth the vast majority of high-alumina (HA) mare basalts in the sample collection, although at least one HA basalt from each of Apollo 12 and Apollo 16 have also been identified (Nyquist et al., 1981; Zeigler et al., 2006). They are an important subset of the mare basalt sample collection for several reasons, most importantly their relatively high abundance of Al₂O₃ (~11–16 wt% Al₂O₃) compared to other mare basalts (7–11 wt% Al₂O₃) (Albee et al., 1972; Grieve et al., 1972; Helmke and Haskin, 1972; Ridley, 1975; Kurat et al., 1976; Ma et al., 1979; Shervais et al., 1985; Dickinson et al., 1985; Neal et al., 1988). This unique chem-

istry and mineralogy describe a petrogenesis different from other mare basalts in that their sources contained a significant amount of plagioclase (e.g., Ridley, 1975; Neal and Kramer, 2006). This in turn has broader implications on the efficiency of plagioclase separation in the Lunar Magma Ocean (LMO) (Taylor and Jakes, 1974; Snyder et al., 1992; Shearer and Papike, 1999) and evolution of the lunar mantle.

Some of the HA basalts sampled by Apollo 14 represent the oldest mare basalt eruptions (~4.25 Ga) (e.g., Dasch et al., 1987), predating the main sequence of mare volcanism that filled the great lunar basins. The combined Apollo 14 and Luna 16 sample collection demonstrates that the duration of aluminous mare volcanism lasted at least 1 billion years (e.g., Nyquist et al., 1981; Dasch et al., 1987; Nyquist and Shih, 1992; Snyder et al., 2000; Cohen et al., 2001). Aluminous basalt fragments have been sampled from regions separated by ~2400 km. Their range in age, location, and variation in geochemistry suggests that HA basalts may be more common than previously thought. They may be a

* Corresponding author at: Bear Fight Center, 22 Fiddler's Rd, Winthrop, WA 98862, USA.

E-mail address: gkramer@bearfightcenter.com (G.Y. Kramer).

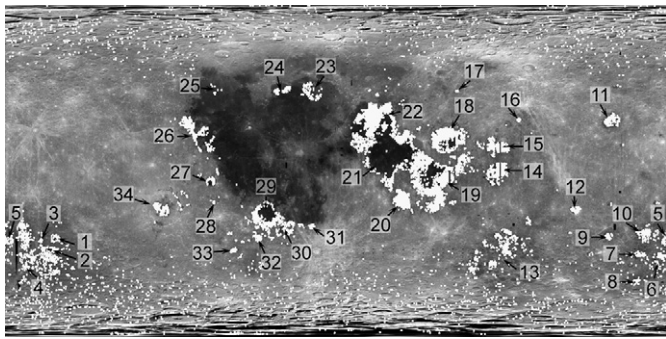


Fig. 1. Clementine 750 nm base map at 1 km resolution. White areas depict intersection of compositional constraints based on HA sample data: 12–18 wt% FeO, 1–5 wt% TiO₂, and 0–4 ppm Th. FeO compositional data based on algorithms of Lucey et al. (2000b) and Wilcox et al. (2005) from Clementine data at 100 m/pixel. TiO₂ compositional data from algorithm of Lucey et al. (2000b) from Clementine data at 250 m/pixel. Th data from LP-GRS (Prettyman et al., 2002) at half degree/pixel resolution. Numbers correspond to ROIs identified in Table 1.

significant component of ancient basalts and could be related to cryptomare (Schultz and Spudis, 1979; Hawke et al., 2005a, 2005b).

Knowing the extent of aluminous basaltic volcanism would be another step toward understanding the nature and history of the Moon. The aluminous nature of these basalts results from one of three scenarios:

- (1) Assimilation of the anorthositic crust by a (low-alumina) mare basalt magma,
- (2) Mixing of (low-alumina) mare basalt with anorthositic crust by impact-induced melt, or
- (3) Plagioclase retained in the source.

Neal and Kramer (2006) addressed all three scenarios, with focus on a model of the petrogenesis of the Apollo 14 HA basalts. Their conclusions favored scenario 3, and provided evidence against scenarios 1 and 2 (see also Finnila et al., 1994; Ridley, 1975; Warren et al., 1997; Hagerty et al., 2005). Thus, the evidence for plagioclase retained in the source of the HA basalts implies that plagioclase flotation was inefficient during the differentiation of the LMO, and that some plagioclase remains within the uppermost lunar mantle. Another, although less likely scenario of an Al-rich source, is from spinel or garnet in the source. In this case, the basalts must be derived from much greater depths (i.e., >500 km for garnet). Spinel could be the aluminous phase between 250 and 500 km within the lunar mantle (Neal, 2001).

In a previous paper (Kramer et al., 2008), we described a method for identifying potential HA basalt exposures on the lunar surface using Clementine multispectral and Lunar Prospector gamma-ray spectrometer (LP-GRS) data. Compositional parameters for the Moon-wide search were based on known compositions from HA basalt samples and were used to map the distribution of HA basalts globally (12–18 wt% FeO, 1.5–5 wt% TiO₂, and 0–4 ppm Th, Fig. 1, Table 1). Selected regions of interest (ROIs) were more closely evaluated using high-resolution (100 m/pixel) FeO and TiO₂ compositional data derived from the Clementine multispectral camera. In our previous work, we characterized the mare basalt units of two of these ROIs: Mare Moscovense and Mare Nectaris, and concluded that each basin contained at least one basalt unit consistent with a HA composition (see Kramer et al., 2008). The current paper focuses on two other ROIs highlighted in Fig. 1: Northern Mare Imbrium (Sinus Iridum and South of Plato) and Mare Fecunditatis. They were selected because they are the likeliest candidates for the source of the HA basalts sampled by Apollo 14 and Luna 16.

Table 1
ROIs highlighted by compositional constraints

| | ROI | Lat | Lon |
|----|------------------------------|-----|------|
| 1 | Apollo (center) | 36S | 153W |
| 2 | Apollo (lower between rings) | 43S | 155W |
| 3 | Oppenheimer | 46S | 168W |
| 4 | Bose | 55S | 167W |
| 5 | Leibnitz | 39S | 179E |
| 6 | Von Karmen | 46S | 174E |
| 7 | Chretien | 45S | 161E |
| 8 | Poincaré | 58S | 162E |
| 9 | Jules Verne | 35S | 146E |
| 10 | Mare Ingenii | 34S | 168E |
| 11 | Mare Moscovense | 27N | 146E |
| 12 | Tsiolkovskiy | 20S | 129E |
| 13 | Mare Australe (areas) | 42S | 90E |
| 14 | Mare Smythii | 2N | 89E |
| 15 | Mare Marginis | 14N | 87E |
| 16 | Lomonosov | 28N | 98E |
| 17 | Lacus Spei | 43N | 65E |
| 18 | Mare Crisium | 18N | 60E |
| 19 | Mare Fecunditatis | 3S | 51E |
| 20 | Mare Nectaris | 16S | 35E |
| 21 | Mare Tranquillitatis | 9N | 31E |
| 22 | Mare Serenitatis | 25N | 19E |
| 23 | South of Plato | 43N | 13W |
| 24 | Sinus Iridum | 44N | 30W |
| 25 | E. Sinus Roris | 44N | 64W |
| 26 | W. Proc (Struve) | 20N | 74W |
| 27 | Grimaldi | 6S | 68W |
| 28 | Cruger | 17S | 67W |
| 29 | Humorum | 23S | 40W |
| 30 | Palus Epidemiarum | 31S | 32W |
| 31 | Pitatus | 30S | 13W |
| 32 | Lacus Excellentiae | 35S | 42W |
| 33 | Lacus Excellentiae West | 43S | 56W |
| 34 | Mare Orientale | 20S | 95W |

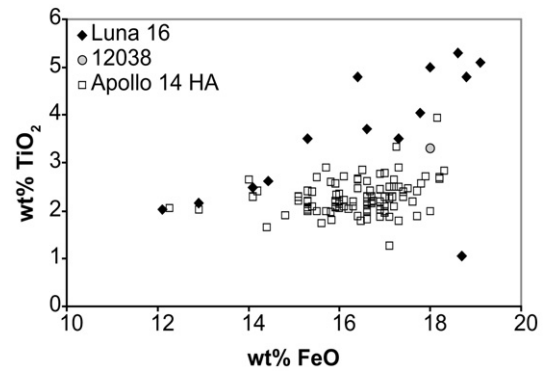


Fig. 2. Wt% FeO versus wt% TiO₂ for HA mare basalt samples. Data sources: Luna 16: Jakes et al. (1972), Kurat et al. (1976), Ma et al. (1979); Apollo 12: Reid and Jakes (1974); Apollo 14: Ehmann et al. (1972), Hubbard et al. (1972b), Lindstrom et al. (1972), Longhi et al. (1972), Strasheim et al. (1972), Taylor et al. (1972), Ridley (1975), Shervais et al. (1985), Dickinson et al. (1985), Neal et al. (1988, 1989), Neal and Taylor (1989).

1.1. Luna 16

Luna 16 landed on the northeastern corner of Mare Fecunditatis on September 20, 1970. The robotic mission returned to Earth with a small drill core of the surface regolith comprised of ~20% basaltic fragments (Reid et al., 1972). Virtually all of these basalts have a HA composition (Kurat et al., 1976). Compared to the Apollo 14 basalts, some Luna 16 HA basalts have a greater variation in TiO₂ abundance (up to 5 wt%, Fig. 2), Al₂O₃ (11–20 wt% Al₂O₃), and lower Mg# (between 0.3 and 0.4) than Apollo 14 HA basalts (Vinogradov, 1971; Kurat et al., 1976; Ma et al., 1979; Taylor et al., 1991). The lower Mg# (due to lower MgO) suggests these basalts derived from more evolved LMO cu-

mulates than did the Apollo 14 HA basalts (Kurat et al., 1976). Luna 16 HA basalts have a greater abundance of light REE compared to the heavy REE, resulting in a slightly bow-shaped chondrite-normalized rare earth element (REE) profile (Taylor et al., 1991). Radiometric ages of the Luna 16 basalts indicate at least three eruptive episodes occurring between 3.42 and 3.15 Ga (Huneke et al., 1972; Cadogen and Turner, 1977; Fernandes et al., 2000; Cohen et al., 2001), erupting contemporaneously with other, low-alumina mare basalts. The unique chemistry and proportions of particle types in the Luna 16 regolith sample suggests the source material was derived from local areas (Hubbard et al., 1972a), and thus implies that at least a portion of Mare Fecunditatis is dominated by aluminous mare basalts.

1.2. Apollo 14

In February, 1971, Apollo 14 returned to Earth with a collection of samples from the Fra Mauro formation, a promontory in Oceanus Procellarum that marks the eastern boundary of Mare Cognitum. Fra Mauro is formed of ejecta deposits from the Imbrium impact (~3.85 Ga) (Wilhelms, 1987). Among the samples collected during this mission were several HA mare basalts. They came predominately in the form of clasts in breccia 14321 (e.g., Grieve et al., 1975; Duncan et al., 1975), although there are two HA specimens that are not part of any breccia, samples 14053 and 14072 (Papanastassiou and Wasserburg, 1971; El Goresy et al., 1972). The Apollo 14 HA basalts, therefore, are probably not indigenous to that region, but rather originated from the Imbrium region prior to basin formation.

All of the Apollo 14 HA basalts are low-Ti (1.5–4 wt% TiO₂, Fig. 2) and exhibit relatively minor variation in major element chemistry. Other relevant major-element oxide abundances of HA basalts sampled by this mission are: 13–19 wt% FeO, 11–16 wt% Al₂O₃, and Mg# between 0.4 and 0.55. Major element chemistry suggests this collection could be modeled by simple, closed-system fractional crystallization (Dickinson et al., 1985). However, there are two features of this collection that complicate the matter of their petrogenesis, and require a more complex explanation than simple fractional crystallization: (1) most Apollo 14 HA basalts are light rare earth element (LREE) enriched to varying degrees; and (2) they vary substantially in their incompatible trace element abundance, demonstrating an eight-fold increase between the lowest and highest abundances. Radiometric ages indicate at least three, and possibly four distinct ages ranging between 3.9 and 4.3 Ga, which predate and are contiguous with the beginning of extensive mare volcanism, which marks the upper Imbrian (~3.9 Ga) (Papanastassiou and Wasserburg, 1971; Taylor et al., 1983; Dasch et al., 1987; Wilhelms, 1987; Shih and Nyquist, 1989a, 1989b). Modeling of their trace element compositions implicates KREEP as a component in the source (Hughes et al., 1990) and in some cases during ascent and crystallization (Neal et al., 1988). Isotopic and trace element data are consistent with the age groups, indicating that the Apollo 14 HA basalts were derived from trace-element distinct source regions, and at different times (Neal and Kramer, 2006).

2. Data and analysis

The reader is referred to Kramer et al. (2008) for a detailed explanation of the methodology. A brief summary is given here. The method uses compositional remote sensing data constrained by known sample compositions to find regions on the lunar surface where HA mare basalts appear to have erupted. Three data sets are used to achieve this end:

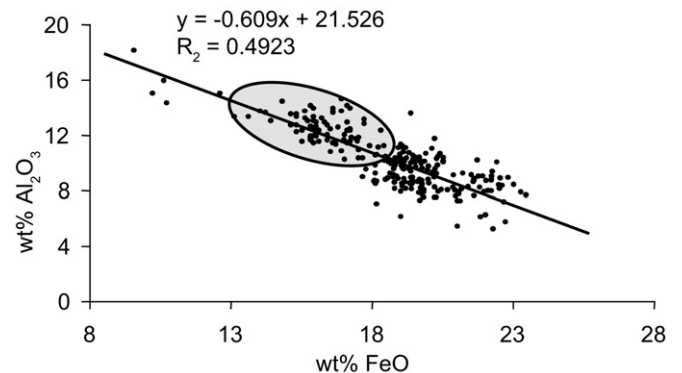


Fig. 3. Inverse correlation of Al₂O₃ and FeO for mare basalt samples (the relationship does extend to highland samples) allows the use of FeO as a proxy for Al₂O₃ in the search for high-Al basalts using remote sensing. Circled region depicts HA mare basalts. Four lower-FeO data points are a subclass of HA basalts—the VHK basalts, not included due to their deviant characteristics. Data from Neal (2006).

- (1) LP-GRS thorium abundances (Prettyman et al., 2002),
- (2) Clementine-derived TiO₂ (Lucey et al., 2000b),
- (3) and Clementine-derived FeO abundances (Wilcox et al., 2005).

Clementine image cubes were processed using ISIS (Integrated Software for Imaging Spectrometers) (Eliason, 1997). For the whole-Moon search, Clementine data was coregistered and resampled to match the LP-GRS projection and resolution (0.5 degree/pixel). The white regions in Fig. 1 represent HA compositions on the lunar surface, and result from the intersection of three masks, or filters, that pass the constraints for a HA basalt, based on the Apollo 14 and Luna 16 returned samples. The constraints are: 12–18 wt% FeO, 1.5–5 wt% TiO₂, and 0–4 ppm Th. FeO values slightly exceed the range of sample compositions to account for the influence of adjacent lithologies on regolith composition. Nevertheless, these constraints do assume that HA basalts dominate the regolith by contributing at least 70% to its composition (Kramer et al., 2008).

Ideally, we would include Mg and (obviously) Al in these data sets, however the resolutions of the available elements (from LP-GRS) do not exceed 5 degrees/pixel (Feldman et al., 1999). Distinguishing mare-highland mixtures from surfaces underlain by aluminous basalts, and particularly discerning different mare basalt types that fill a basin, is not practical at this resolution. Despite this, we can still make reasonable assessments utilizing the inverse relationship between FeO and Al₂O₃ for mare basalts (Fig. 3). This relationship reflects the basalts' mineralogy; and in the case of the HA basalts corresponds to high modal proportions of plagioclase (increased Al₂O₃) and lower pyroxene and olivine (decreased FeO) (cf. Papike et al., 1974).

Selected ROIs identified with the HA constraint map (Fig. 1, Table 1) are examined in greater detail using high-resolution (100 m/pixel) Clementine 5-band UV-VIS-NIR image cubes. FeO compositional images (Figs. 6c, 9c) were created using the algorithms of Lucey et al. (2000b) ($\sigma = 1.1$) for FeO < 10 wt% and Wilcox et al. (2005) ($\sigma = 0.5$) for FeO > 10 wt%. TiO₂ compositional images were derived from the algorithm of Lucey et al. (2000b) ($\sigma = 1.0$; Figs. 6d, 9d). Mare basalt unit compositions are estimated from pixels that depict the rims and proximal ejecta of small craters (0.4–4 km in diameter) that impacted into the unit. These small craters act as windows through the ubiquitous, obscuring regolith, exposing the underlying, uncontaminated mare basalt (McCord and Adams, 1973; Staid and Pieters, 2000). Our rationale for choosing to focus on the rim and proximal ejecta is based on the impact cratering studies and analysis of impact ejecta mechanics, which demonstrate that the crater ejecta reflects the stratigraphy of the impact target, that is, inverted (Melosh, 1989).

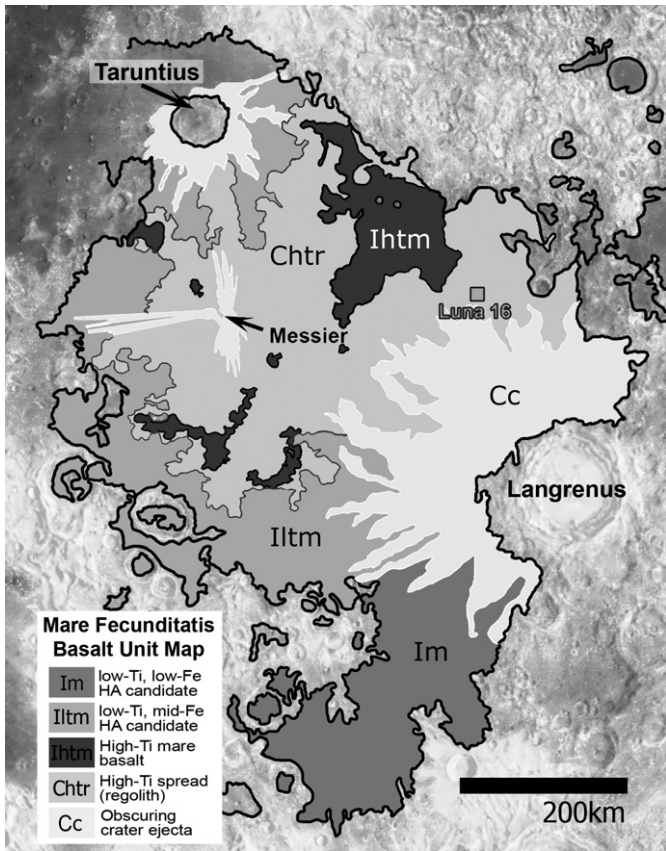


Fig. 4. Map of Fecunditatis depicting major compositional units.

Therefore, this region, being the thickest part of the crater ejecta, exposes the subsurface stratigraphy, and being the topographic maximum of the impact structure, provides the best estimate of the composition of the basaltic unit underlying the obscuring regolith.

3. Analytical results

This paper reports our analyses of two ROIs, selected from the constraint map (Fig. 1) to be the likely source regions of HA basalts sampled by the Apollo 14 and Luna 16 missions. We use the word “source” here to mean the selenographic position on the lunar surface where the HA basalts erupted, flowed, and crystallized, not specifically the mantle source for the basalts. Although, erupted lava flows can be considered the surface expression of a vertical column to the mantle source. Since HA basalts sampled by Luna 16 are considered indigenous to the landing site, Mare Fecunditatis was the logical choice of locations highlighted on the HA constraint map (#19, Fig. 1). It is apparent in Fig. 1 that the Fra Mauro region, the landing site of Apollo 14, was not selected by the compositional constraints. This is not surprising since the Fra Mauro formation is recognized as ejecta from the Imbrium impact (Wilhelms, 1987). We would therefore expect the source of the Apollo 14 HA basalts to be in Imbrium. Fig. 1 shows two ROIs (#s 23 & 24) in northern Mare Imbrium that we consider the plausible candidates for the Apollo 14 HA source.

The ubiquitous regolith is composed mostly of underlying and immediately adjacent lithologies, but also contains a significant fraction of material from more exotic locations. The contribution of exotic materials to a given location increases with increased maturity of the location. The OMAT index does not directly correlate with age, however it is useful when evaluating the basalt units. Craters used in this study are limited to those with an op-

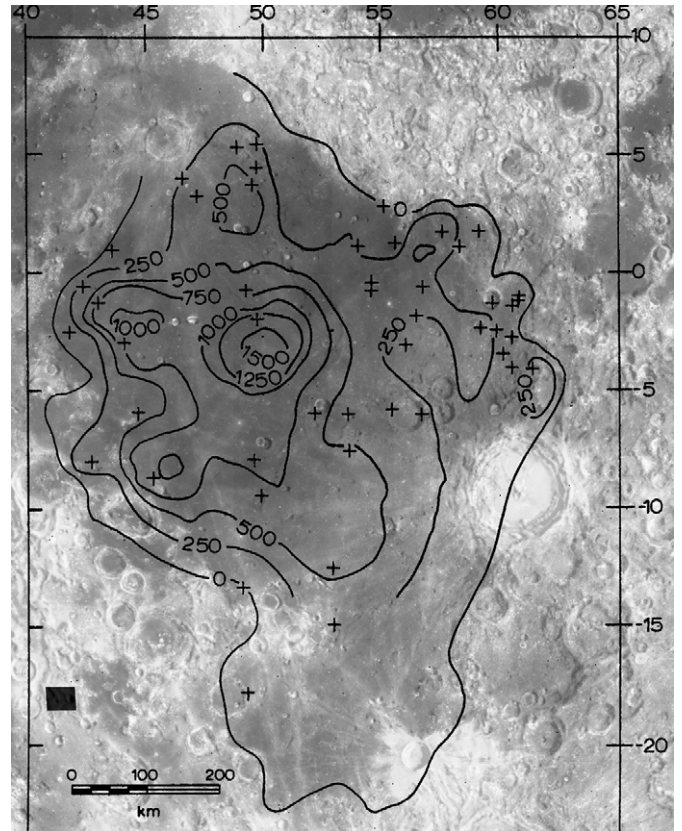


Fig. 5. Isopach map of mare thickness from DeHon (1975) overlain on combined Clementine 750 nm and shaded relief.

tical maturity (OMAT) index (cf. Lucey et al., 2000a) of > -0.90 for Northern Mare Imbrium and > -0.93 for Mare Fecunditatis. These values were chosen to restrict our analyses to “fresh” ejecta deposits while ensuring a representative sample distribution. The OMAT can also be used for estimating the composition of regolith produced and deposited atop an analyzed small crater after its formation based on the increasing diameter of a “circle of influence” from adjacent lithologies (Kramer et al., 2008).

3.1. Mare Fecunditatis

We present two arguments to demonstrate that we can identify HA basalts in Mare Fecunditatis (#19 in Fig. 1): (1) the samples brought to Earth by Luna 16 established the presence of HA basalts in the region; and (2) our analysis of the region showed that impacts that penetrated the regolith exposed compositions consistent with the Luna 16 HA sample chemistry. The basalt unit map for Mare Fecunditatis (Fig. 4) depicts the distribution of the different basaltic units that fill the basin based on the results of this analysis. The map does not distinguish every flow unit, as does Rajmon and Spudis (2004), nor is it intended to resemble a comprehensive geologic map. The map portrays the mare divided into different basalt units based on major Clementine-derived compositional variations from this study, and/or ages from crater counting statistics of previous workers (Boyce, 1976).

Fecunditatis is an old, pre-Nectarian basin filled with basalts middle- to late-Imbrian in age (Wilhelms, 1987). Basalt thickness averages 500 m (Rajmon and Spudis, 2004), with estimated local depths as great as 1500 m (Fig. 5) (DeHon, 1975). The age of basalt fill is estimated at middle- to late-Imbrian (Pieters, 1978; Wilhelms, 1987). The mare surface is complex owing to the crossing of numerous large-scale ejecta deposits. These impacts excavated deep into the highland crust, depositing thick layers of

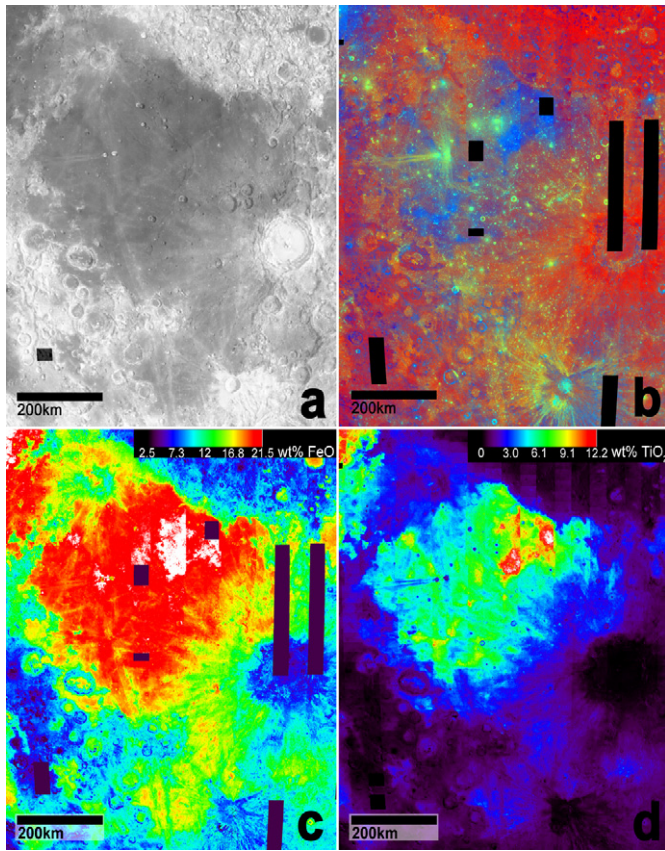


Fig. 6. Clementine imagery for Mare Fecunditatis. (a) 750 nm reflectance, (b) Clementine color ratio composite ($R = 750/415$ nm, $G = 750/950$ nm, $B = 415/750$ nm), (c) FeO (Lucey et al., 2000b; Wilcox et al., 2005), (d) TiO₂ (Lucey et al., 2000b).

low-Fe ejecta over much of the mare. In the path of their ejecta the regolith composition contains a substantially higher amount of non-mare material than other portions of the mare, contributing another obstacle for this analysis. To mitigate a possibly erroneous characterization of the underlying basalt unit, we elected to map those areas as obscuring ejecta blankets, avoiding unjustified speculation.

The regolith composition over Mare Fecunditatis varies with proximity to large-impact ejecta and the young, high-Ti unit (Iltm in Fig. 4). FeO ranges between 17 and 20 wt% in the main, northern basin and between 14 and 17 wt% in the southern tail (Fig. 6c). TiO₂ ranges does not drop below 3 wt% except in the southern tail of Fecunditatis (Fig. 6d). While low-Fe, large-impact ejecta contributes to the regolith composition, the surface of the main basin is strongly influenced by a high-Ti unit.

3.1.1. Low-Fe, low-Ti unit: Im

Several impacts as small as 2.5 km in diameter into unit Im have very low-Fe ejecta (6–11 wt% FeO), suggesting they exposed the basin floor, and thus leading to the interpretation that unit Im is relatively thin. Near its northern-most boundary, larger impacts indicate the unit may be as thick as 500 m, but most of unit Im is less than 250 m thick. These estimates are consistent with thickness estimates of DeHon (1975). The range in FeO abundances from small, immature impacts into this unit are broad (6–16 wt% FeO), less so than TiO₂ (1–3 wt%, Table 2). The unique range in compositions measured in the ejecta of small impacts into unit Im is explained if the lower portion of Fecunditatis is only filled with Im flows. Since Im is not adjacent to high-Ti, high-Fe units, the only influence on the composition of the regolith atop small-crater

Table 2

Mean compositions and maturity of small craters in Mare Fecunditatis' basalt units Im

| FeO | TiO ₂ | OMAT | FeO | TiO ₂ | OMAT | FeO | TiO ₂ | OMAT |
|--------------------------|------------------|--------|------|------------------|--------|------|------------------|--------|
| 0.4–1 km diameter | | | | | | | | |
| 12.4 | 1.3 | -0.867 | 14.9 | 2 | -0.893 | 15.7 | 2.6 | -0.918 |
| 14.4 | 2 | -0.872 | 6.4 | 1.1 | -0.896 | 14.5 | 1.9 | -0.919 |
| 14.7 | 1.8 | -0.874 | 13.5 | 1.7 | -0.896 | 12 | 1.4 | -0.92 |
| 7.9 | 0.9 | -0.875 | 13.2 | 1.1 | -0.896 | 14.4 | 2.4 | -0.921 |
| 14.4 | 1.7 | -0.875 | 13.2 | 1.6 | -0.897 | 7.2 | 1.6 | -0.921 |
| 15.6 | 1.7 | -0.876 | 8.7 | 1.7 | -0.897 | 15.2 | 2.5 | -0.922 |
| 12.3 | 1.4 | -0.876 | 15.5 | 2.6 | -0.901 | 14.8 | 2.3 | -0.923 |
| 13.6 | 1.8 | -0.879 | 11 | 1.4 | -0.905 | 14.6 | 2 | -0.924 |
| 8.1 | 1 | -0.88 | 13.5 | 1.3 | -0.906 | 15.2 | 3.5 | -0.925 |
| 13.5 | 1.7 | -0.881 | 14.6 | 2 | -0.907 | 15 | 2.2 | -0.927 |
| 13.5 | 1.8 | -0.885 | 13.9 | 1.9 | -0.907 | 12.3 | 1.8 | -0.927 |
| 13.3 | 1.5 | -0.885 | 13 | 1.7 | -0.91 | 8.8 | 1.6 | -0.928 |
| 14.3 | 1.9 | -0.887 | 14.6 | 2.3 | -0.913 | 14.2 | 2 | -0.929 |
| 11.6 | 1.3 | -0.887 | 10.4 | 1.2 | -0.913 | 14.9 | 2.4 | -0.931 |
| 13.8 | 1.4 | -0.889 | 14.8 | 2.2 | -0.914 | 15.5 | 3.3 | -0.935 |
| 14 | 2 | -0.889 | 13.6 | 1.5 | -0.916 | 13.3 | 1.4 | -0.937 |
| 11.4 | 1.2 | -0.889 | 11.4 | 1.4 | -0.916 | 7.3 | 1.1 | -0.938 |
| 14.1 | 1.6 | -0.891 | 14.2 | 1.7 | -0.916 | 14.2 | 1.7 | -0.938 |
| 14.3 | 1.8 | -0.893 | 15.8 | 2.7 | -0.917 | 14.7 | 2.5 | -0.941 |
| 1–2 km diameter | | | | | | | | |
| 11 | 0.8 | -0.797 | 14.8 | 1.5 | -0.891 | 11.4 | 1.4 | -0.922 |
| 12.7 | 1.2 | -0.815 | 15.7 | 2.7 | -0.891 | 14 | 1.8 | -0.924 |
| 13.8 | 1.3 | -0.817 | 6.9 | 1.1 | -0.892 | 14.7 | 2.3 | -0.925 |
| 12.6 | 1.2 | -0.837 | 13.1 | 1.4 | -0.897 | 15.1 | 1.8 | -0.925 |
| 15.2 | 2 | -0.854 | 6.9 | 1.8 | -0.9 | 15.6 | 2.7 | -0.926 |
| 15.2 | 1.9 | -0.856 | 15.3 | 2.1 | -0.9 | 14.7 | 2 | -0.927 |
| 15.9 | 2.4 | -0.857 | 12.8 | 1.2 | -0.901 | 13.3 | 1.7 | -0.927 |
| 15.7 | 2.1 | -0.861 | 14.9 | 1.9 | -0.909 | 15.3 | 2.2 | -0.929 |
| 7.5 | 1 | -0.863 | 15.4 | 2.4 | -0.91 | 14.6 | 1.8 | -0.93 |
| 15.1 | 2.1 | -0.863 | 14.3 | 2 | -0.91 | 13.7 | 1.9 | -0.93 |
| 15.6 | 2.3 | -0.865 | 14.4 | 1.8 | -0.91 | 14 | 1.6 | -0.931 |
| 14.9 | 2 | -0.867 | 14.6 | 1.7 | -0.911 | 14.8 | 2 | -0.932 |
| 15.1 | 1.7 | -0.869 | 13 | 1.6 | -0.912 | 13.9 | 2.1 | -0.933 |
| 14.7 | 1.8 | -0.874 | 14.7 | 1.8 | -0.913 | 14.7 | 2 | -0.934 |
| 14.4 | 1.7 | -0.879 | 15.5 | 2.5 | -0.914 | 14.8 | 2.3 | -0.94 |
| 15.5 | 2.2 | -0.879 | 12.5 | 1.8 | -0.916 | 14.9 | 2 | -0.941 |
| 14.3 | 2.1 | -0.88 | 14.6 | 2.4 | -0.918 | 13.2 | 1.8 | -0.941 |
| 15 | 2 | -0.885 | 13.5 | 1.7 | -0.918 | 10.1 | 1.7 | -0.943 |
| 10.9 | 1.1 | -0.889 | | | | | | |
| 2–3 km diameter | | | | | | | | |
| 15.4 | 2.4 | -0.868 | 14.6 | 1.9 | -0.902 | 14.1 | 2.2 | -0.941 |
| 12.9 | 1.6 | -0.881 | | | | | | |
| 3–4 km diameter | | | | | | | | |
| 14.5 | 2 | -0.879 | 15.3 | 2.6 | -0.913 | | | |

ejecta would come from Langrenus ejecta, the surrounding highlands, and the basin floor. We conclude that the composition of Im must be reflected in the upper limit of its range, and estimate it to be between 14 and 16 wt% FeO and 1.5 and 3 wt% TiO₂. Unit Im is certainly within the constraints for a HA basalt, however its FeO and TiO₂ abundances do not reflect the composition of the basalts sampled by Luna 16.

3.1.2. Mid-Fe, low-Ti unit: Iltm

Mare basalt flows that make up unit Iltm fill the main basin, but stop short of completely covering unit Im in the lower portion of Fecunditatis. Unit Iltm and its Ti-rich spread, Chtr, cover a large portion of Iltm, although Iltm's chemical signature is evident in even the smallest impacts into Iltm and Chtr, as well as in ejecta blankets from Taruntius and Langranus. The precise delineation of Iltm's boundaries is complicated by the obscuring regolith mapped as Chtr, ejecta from Langrenus and Taruntius, and unit Iltm's intermediate composition between units Iltm and Im. We are certain that unit Iltm is a distinct basalt unit, and we have determined that its composition is best represented by the grouping of the larger craters (between 2 and 4 km in diameter) in Fig. 7. These craters

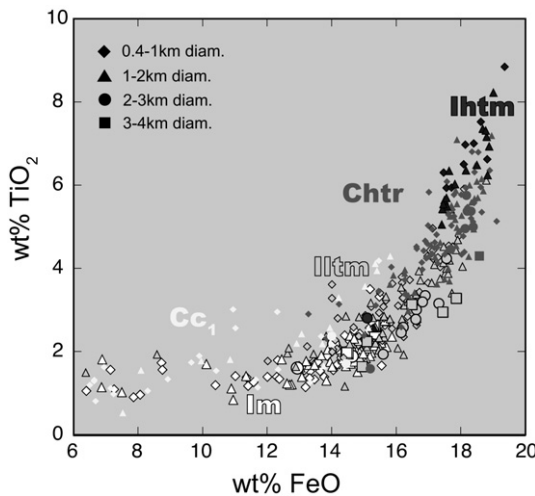


Fig. 7. FeO vs TiO₂ for rims and proximal ejecta of small impacts into Mare Fecunditatis.

represent some of the least mature impacts available for analysis in the region. Excavation depth of a crater is related to its diameter (e.g., Melosh, 1989), and these craters' diameters indicate they were sufficient to penetrate the regolith, excavating deep into the target basalt. These large craters also demonstrate the uniformity of unit Iltm with depth. We estimate the composition of unit Iltm to be between 16–18 wt% FeO and 3–4 wt% TiO₂. The composition of this unit, as well as its location, make this unit the best candidate for the source of the Luna 16 HA basalts.

The distribution of crater ejecta compositions into unit Iltm (Fig. 7) could be used to argue that some of the impacts are sampling a deeper, different unit, probably unit Im. This is possible, and even likely since unit Im is slightly older than Iltm, and probably flowed further in the basin than is evident from its currently visible extent. However, there is no correlation between crater size and composition for impacts into unit Iltm (Table 3) to support this interpretation. We have therefore not attempted to map the sub-Iltm extent of unit Im.

3.1.3. High-Fe, high-Ti unit: Iltm

Iltm is the high-Ti unit exposed in at least 3 locations in Fecunditatis. It is likely that Iltm was at one time a single coherent unit, that has been dispersed by impact gardening, leaving only its thickest portions as evidence of its previous boundaries. Superposition dictates that Iltm is the youngest unit in Fecunditatis. As the youngest unit in the basin, it also marks the end of volcanic activity into Fecunditatis, identified as upper Imbrian by Pieters (1978) and Wilhelms (1987). Most impacts into this unit reveal compositions between 18–21 wt% FeO and 5–9 wt% TiO₂ (Table 4). The narrow range in FeO, and wide range in TiO₂ testifies to the influence of an underlying unit, with a significantly contrasting Ti abundance, but only slightly different FeO abundance. Langrenus or Taruntius ejecta is rejected as a contaminating influence in this case for two reasons: (1) the small craters used in our analyses are selected for their low OMAT value, and therefore would postdate the Langrenus or Taruntius impact events, and (2) the ejecta composition is dominated by the highlands lithology, which would have had a more pronounced effect on the FeO as well TiO₂. Evidence for an underlying, low-Ti basalt unit is supported by larger impacts into Iltm that expose significantly lower FeO and TiO₂ (Fig. 7). These impacts appear to have completely penetrated Iltm and are exposing the underlying unit.

Although the ejecta of small impacts into unit Iltm display a wide range in compositions, we interpret the composition of the unit itself to be reflected in the upper limits of this range, since

Table 3

Mean compositions and maturity of small craters in Mare Fecunditatis' basalt unit Iltm

| FeO | TiO ₂ | OMAT | FeO | TiO ₂ | OMAT | FeO | TiO ₂ | OMAT |
|--------------------------|------------------|--------|------|------------------|--------|------|------------------|--------|
| 0.4–1 km diameter | | | | | | | | |
| 12 | 1.8 | -0.865 | 17 | 3.7 | -0.906 | 14 | 2.1 | -0.924 |
| 14.1 | 2.3 | -0.873 | 15.6 | 3.1 | -0.907 | 15.2 | 2.6 | -0.924 |
| 16.6 | 2.6 | -0.882 | 15.5 | 2.9 | -0.909 | 17.8 | 4.5 | -0.925 |
| 16.7 | 3.2 | -0.883 | 17.1 | 5 | -0.912 | 16.7 | 3.4 | -0.926 |
| 16.7 | 2.7 | -0.886 | 15.9 | 2.6 | -0.912 | 16.2 | 3.3 | -0.926 |
| 16.2 | 2.4 | -0.886 | 14.8 | 2.4 | -0.914 | 15 | 2.9 | -0.926 |
| 15.6 | 2.8 | -0.889 | 14 | 3.6 | -0.915 | 17.2 | 4.2 | -0.927 |
| 15.6 | 2.3 | -0.89 | 15.3 | 2.6 | -0.916 | 14 | 2 | -0.928 |
| 16.5 | 3.3 | -0.892 | 17.1 | 4.4 | -0.918 | 18.1 | 5.9 | -0.931 |
| 16.7 | 3.4 | -0.895 | 17.6 | 4.5 | -0.918 | 15.7 | 3.2 | -0.932 |
| 14.2 | 2.8 | -0.896 | 13.2 | 2.1 | -0.918 | 16.2 | 3.3 | -0.933 |
| 17.6 | 4.2 | -0.896 | 15.3 | 2.6 | -0.918 | 14.2 | 2.1 | -0.934 |
| 16.3 | 2.7 | -0.896 | 17.4 | 4 | -0.921 | 17 | 4.3 | -0.935 |
| 16.1 | 3.1 | -0.899 | 16.2 | 3.5 | -0.921 | 16.2 | 3.8 | -0.935 |
| 16.2 | 3.7 | -0.899 | 15.2 | 3.1 | -0.922 | 16.4 | 2.8 | -0.936 |
| 14.4 | 1.9 | -0.902 | 14.7 | 2.6 | -0.922 | 17.3 | 4.3 | -0.937 |
| 17.9 | 4.8 | -0.903 | 14 | 3.3 | -0.922 | 17.1 | 4.4 | -0.937 |
| 16.4 | 3.7 | -0.904 | 15.5 | 3.4 | -0.923 | 15.9 | 3.6 | -0.943 |
| 1–2 km diameter | | | | | | | | |
| 14.4 | 1.2 | -0.79 | 17.5 | 4.1 | -0.895 | 15.8 | 2.8 | -0.92 |
| 16.2 | 1.9 | -0.844 | 16.6 | 3.4 | -0.895 | 17.5 | 4.5 | -0.92 |
| 15.5 | 2.1 | -0.858 | 17.9 | 4.4 | -0.899 | 8.6 | 1.9 | -0.921 |
| 16.1 | 2.1 | -0.86 | 15 | 1.7 | -0.901 | 17.1 | 4.3 | -0.921 |
| 17.7 | 3.4 | -0.861 | 15.1 | 2.3 | -0.904 | 17.6 | 4 | -0.922 |
| 18.1 | 4 | -0.867 | 12.9 | 1.6 | -0.904 | 14.9 | 2.8 | -0.922 |
| 15.6 | 2.4 | -0.867 | 13.8 | 2.4 | -0.904 | 12.7 | 2.1 | -0.923 |
| 17.4 | 3.8 | -0.868 | 13.4 | 1.9 | -0.905 | 15.5 | 2.3 | -0.924 |
| 6.4 | 1.5 | -0.876 | 16.7 | 3.9 | -0.91 | 17.5 | 3.9 | -0.924 |
| 15.5 | 2 | -0.881 | 16.1 | 2.6 | -0.911 | 16.4 | 3.2 | -0.924 |
| 15.6 | 2.3 | -0.881 | 17.7 | 4.2 | -0.912 | 17.9 | 4.7 | -0.926 |
| 17.6 | 3.9 | -0.885 | 15.3 | 2.8 | -0.912 | 14.6 | 2.2 | -0.928 |
| 16.8 | 3.7 | -0.888 | 17.2 | 4.1 | -0.913 | 14.4 | 2.9 | -0.929 |
| 15.1 | 2.1 | -0.889 | 15.4 | 2.2 | -0.913 | 17.7 | 5.4 | -0.931 |
| 17.1 | 3.7 | -0.89 | 16.3 | 3.1 | -0.915 | 15.2 | 3.2 | -0.931 |
| 16.2 | 3.5 | -0.891 | 16.2 | 2.8 | -0.916 | 18.8 | 6.1 | -0.931 |
| 15.6 | 2.9 | -0.891 | 15.7 | 3.3 | -0.917 | 18.7 | 6.2 | -0.934 |
| 12.6 | 2 | -0.893 | 15.4 | 2.6 | -0.919 | 17.5 | 5.6 | -0.939 |
| 2–3 km diameter | | | | | | | | |
| 16.2 | 2.5 | -0.851 | 17.3 | 3.2 | -0.873 | 17.6 | 4.2 | -0.897 |
| 15.6 | 1.9 | -0.851 | 16.8 | 3.2 | -0.884 | 16.6 | 2.8 | -0.901 |
| 16.9 | 3.4 | -0.858 | 16.2 | 2.6 | -0.892 | 16.6 | 3 | -0.905 |
| 3–4 km diameter | | | | | | | | |
| 17.4 | 3 | -0.832 | 16.5 | 3.1 | -0.849 | 15.1 | 2.2 | -0.904 |
| 17.9 | 3.3 | -0.849 | 14.9 | 1.6 | -0.882 | | | |

Table 4

Mean compositions and maturity of small craters in Mare Fecunditatis' basalt unit Iltm

| FeO | TiO ₂ | OMAT | FeO | TiO ₂ | OMAT | FeO | TiO ₂ | OMAT |
|--------------------------|------------------|--------|------|------------------|--------|------|------------------|--------|
| 0.4–1 km diameter | | | | | | | | |
| 17.5 | 6.3 | -0.889 | 12.2 | 5.8 | -0.907 | 17.7 | 5.9 | -0.921 |
| 18.1 | 6.5 | -0.899 | 18.8 | 6.6 | -0.919 | 18.6 | 7.5 | -0.922 |
| 17.6 | 5.9 | -0.904 | | | | | | |
| 1–2 km diameter | | | | | | | | |
| 15.3 | 2.6 | -0.803 | 18.9 | 6.9 | -0.898 | 17.8 | 6 | -0.907 |
| 17.4 | 5.1 | -0.86 | 18.8 | 7.2 | -0.899 | 18.2 | 6.4 | -0.91 |
| 17.5 | 5.6 | -0.883 | 18.8 | 6.2 | -0.901 | 18.7 | 7.4 | -0.914 |
| 17.6 | 5.5 | -0.888 | 17.6 | 6.3 | -0.902 | 18.5 | 6.5 | -0.923 |
| 17.5 | 5.5 | -0.892 | 17.6 | 5.7 | -0.902 | 19 | 8.2 | -0.936 |
| 17.4 | 5.4 | -0.895 | 18.8 | 7.3 | -0.903 | | | |
| 2–3 km diameter | | | | | | | | |
| 15.1 | 2.8 | -0.918 | | | | | | |

unit Iltm is the only apparent source of high-Ti and high-Fe. We therefore estimated this unit to have an FeO abundance of close to or greater than 20 wt%, and TiO₂ abundance of at least 8 wt%.

Table 5

Mean compositions and maturity of small craters into Chtr in Mare Fecunditatis

| FeO | TiO ₂ | OMAT | FeO | TiO ₂ | OMAT | FeO | TiO ₂ | OMAT |
|-------------------|------------------|--------|------|------------------|--------|------|------------------|--------|
| 0.4–1 km diameter | | | | | | | | |
| 18.7 | 5.4 | −0.875 | 18.9 | 6.4 | −0.906 | 17.3 | 4.5 | −0.918 |
| 18 | 4.9 | −0.877 | 16.3 | 3.7 | −0.909 | 17.1 | 4.9 | −0.918 |
| 19.1 | 5.1 | −0.877 | 18.8 | 8.6 | −0.909 | 17.2 | 4.5 | −0.918 |
| 15 | 2.4 | −0.881 | 17.8 | 5.8 | −0.91 | 17 | 4.3 | −0.92 |
| 16.8 | 4 | −0.889 | 17.1 | 4.3 | −0.911 | 15.4 | 3.1 | −0.922 |
| 18.2 | 4.9 | −0.889 | 17.6 | 6.1 | −0.912 | 16.9 | 4.7 | −0.922 |
| 16.2 | 2.6 | −0.891 | 16.6 | 4.5 | −0.914 | 13.3 | 2.9 | −0.923 |
| 16.3 | 3.4 | −0.892 | 16.9 | 4.4 | −0.915 | 14.2 | 3.1 | −0.924 |
| 18 | 4.3 | −0.9 | 17.3 | 4.8 | −0.915 | 18.4 | 6.8 | −0.924 |
| 17 | 4.6 | −0.901 | 18.4 | 5.1 | −0.915 | 17 | 5 | −0.924 |
| 18.1 | 4.4 | −0.901 | 17.8 | 5.3 | −0.915 | 15.5 | 3.5 | −0.925 |
| 16.6 | 4.5 | −0.902 | 17.7 | 5 | −0.916 | 18.6 | 6 | −0.925 |
| 17.1 | 4.4 | −0.902 | 18.2 | 5.5 | −0.916 | 16.9 | 4.2 | −0.928 |
| 16.8 | 4.1 | −0.903 | 13.8 | 2.3 | −0.917 | 17.5 | 4.3 | −0.93 |
| 18.1 | 4.8 | −0.903 | | | | | | |
| 1–2 km diameter | | | | | | | | |
| 17.3 | 3.6 | −0.852 | 17.9 | 4.9 | −0.897 | 18.3 | 5.6 | −0.916 |
| 17.7 | 3.7 | −0.853 | 16.3 | 3.4 | −0.902 | 18.4 | 4.9 | −0.919 |
| 17.5 | 3.7 | −0.857 | 18.7 | 5.9 | −0.903 | 16.3 | 3.9 | −0.919 |
| 17.9 | 5.6 | −0.884 | 18.4 | 5.7 | −0.906 | 15.8 | 3.6 | −0.92 |
| 15.9 | 3.8 | −0.887 | 16.4 | 3 | −0.906 | 17.1 | 4.6 | −0.922 |
| 18.3 | 4.3 | −0.888 | 18.5 | 5.7 | −0.907 | 17.8 | 5.2 | −0.922 |
| 18 | 5.3 | −0.888 | 17.9 | 4.5 | −0.908 | 17.7 | 5.3 | −0.923 |
| 17.6 | 4 | −0.89 | 17.2 | 4.3 | −0.912 | 17.9 | 5 | −0.924 |
| 18.5 | 6.1 | −0.892 | 17.8 | 5.9 | −0.912 | 16.4 | 3.4 | −0.925 |
| 18.7 | 6.2 | −0.893 | 17.7 | 5.5 | −0.913 | 18.3 | 6 | −0.925 |
| 17.4 | 4.6 | −0.893 | 17.3 | 4.2 | −0.915 | 17.6 | 4.4 | −0.93 |
| 17.9 | 7.1 | −0.895 | | | | | | |
| 2–3 km diameter | | | | | | | | |
| 15.2 | 1.6 | −0.739 | 18.2 | 5.4 | −0.89 | 18.4 | 5 | −0.907 |
| 18.3 | 5.4 | −0.853 | 18.1 | 5 | −0.899 | 18.2 | 5.8 | −0.924 |
| 17.7 | 4.5 | −0.855 | | | | | | |
| 3–4 km diameter | | | | | | | | |
| 18.6 | 4.3 | −0.851 | | | | | | |

3.1.4. Distinct regolith compositions: Cc and Chtr

On a map intended to depict mare basalt units, we chose to delineate two distinct portions of the mare because of their decided impression on the regolith. If the surface regolith over a location is displaying such a profound influence from a very compositionally distinct lithology, then it is introducing too much complexity to make a reasonable assessment of the underlying mare basalt unit. Despite the careful selection of pixels from the rim and proximal ejecta of each crater, and limiting analyzed craters to those with low maturity, the exposed basalt will always be contaminated with new regolith material deposited since the impact event of the crater under analysis. One cannot ignore the contribution from the smaller, more frequent impacts, whose crater diameter is below than the resolution of Clementine data.

Unit Cc in Fig. 4 depicts the thick ejecta blankets of the Copernican-age craters Taruntius, Langrenus and Messier (Wilhelms, 1987) (Fig. 4). Small, immature impacts into Cc show a correlation between crater size and ejecta composition. Compositions from craters larger than 1 km in diameter plot among the densest grouping of impacts into unit Iltm, while craters smaller than 1 km exhibit lower FeO abundances than the grouping representing unit Im (Fig. 7, Table 5). We interpret this correlation as demonstrating the changing compositions of a vertical column through the low-Fe ejecta blanket of the Copernican craters to the underlying mare basalt unit, Iltm. The crater size required to expose the underlying mare basalt attests to the thickness of the Langrenus ejecta blanket.

Small craters with OMAT parameters > -0.93 into this “unit” consistently expose lower FeO and TiO₂ than the composition of the surrounding surface, demonstrating that Chtr is mostly super-

Table 6

Mean compositions and maturity of small craters into Cc in Mare Fecunditatis

| FeO | TiO ₂ | OMAT | FeO | TiO ₂ | OMAT | FeO | TiO ₂ | OMAT |
|-------------------|------------------|--------|------|------------------|--------|------|------------------|--------|
| 0.4–1 km diameter | | | | | | | | |
| 6.8 | 0.8 | 0.922 | 12.4 | 1.3 | −0.912 | 10.4 | 1.8 | −0.935 |
| 14.3 | 1.2 | −0.844 | 7.4 | 0.9 | −0.919 | 6.6 | 1.1 | −0.935 |
| 12.5 | 1.1 | −0.86 | 13.2 | 2.9 | −0.92 | 7.1 | 1.6 | −0.937 |
| 8.6 | 1 | −0.888 | 11.7 | 2.5 | −0.926 | 11.6 | 3 | −0.939 |
| 5.4 | 0.9 | −0.891 | 14.7 | 2.3 | −0.93 | 9.3 | 1.3 | −0.941 |
| 13.2 | 1.5 | −0.895 | 10.2 | 1.7 | −0.932 | 6.7 | 1.2 | −0.941 |
| 11 | 1.5 | −0.903 | 16.8 | 4.1 | −0.934 | 7.3 | 1.1 | −0.942 |
| 6.8 | 1.3 | −0.905 | | | | | | |
| 1–2 km diameter | | | | | | | | |
| 14.8 | 1.6 | −0.818 | 15 | 3.3 | −0.897 | 13.9 | 2.2 | −0.929 |
| 14.8 | 2.1 | −0.881 | 17.2 | 4.3 | −0.913 | 15.1 | 2.1 | −0.931 |
| 7.8 | 0.5 | −0.881 | 16.7 | 3.9 | −0.914 | 8.4 | 1.5 | −0.932 |
| 16.5 | 2.5 | −0.883 | 11.5 | 1.7 | −0.916 | 14.1 | 2.4 | −0.941 |
| 15 | 2.5 | −0.889 | 16.3 | 3.5 | −0.921 | | | |
| 2–3 km diameter | | | | | | | | |
| 15.5 | 1.7 | −0.846 | 15 | 2.3 | −0.911 | | | |

ficial. In several locations even the smallest craters used in the analysis (400 m) completely penetrate it, and reveal an underlying, distinct, lower-Ti basalt. We interpret this as reflecting the contribution from unit Iltm to the increased TiO₂ abundance of the regolith by impact gardening, while the underlying and adjacent unit Iltm contributes a lower TiO₂ abundance. Ejecta from Langrenus and Taruntius are not considered responsible for the contribution of the lower Ti, because there is no correlating change in composition of small crater ejecta with crater diameter, as was evident in Cc (Fig. 7). Gathered compositions from small crater ejecta span the range from 15–19 wt% FeO and 1.5–7 wt% TiO₂ (Table 6). Based on our analyses of small crater ejecta, we estimate the range of the composition of the exposed unit to: 15–18 wt% and 3–4.5 wt% TiO₂, which is consistent with unit Iltm.

3.2. Northern Mare Imbrium

Impact melt breccias, like those sampled by Apollo 14, are interpreted as having formed from the fragmentation of basaltic rocks by large impacts. These impacts are also responsible for re-consolidation of the basaltic clasts into breccias, with impact melt working as the cement. Since the Fra Mauro Formation is formed of ejecta from the impact that formed the Imbrium basin (Wilhelms, 1987), it is not surprising that the formation itself was not selected as an ROI using the HA compositional constraints for the whole Moon (Fig. 1). We would expect the HA mare basalt source region for the sampled basalts to be either in or near Mare Imbrium. The method did identify the two small regions in Northern Imbrium (#s 23 & 24 in Fig. 1, Table 1) as HA basalt candidates. However, the Imbrium basin is now filled with mare basalt flows that erupted after the Imbrium event (~3.8 Ga), which in turn occurred after the eruption of the sampled HA basalts. If there were any flows that survived basin formation, it would be difficult to find them under hundreds of meters of mare basalt flows that have since filled the basin. We can assume that HA basalts were erupted here in the past, thus demonstrating the presence of a source in the region capable of generating aluminous mare basalts. It is reasonable to assume this source was capable of subsequent eruptions, particularly after de-lamination due to basin formation. So while it is unlikely that we would find the flows from which the sampled Apollo 14 HA basalts originated, our investigation may have located the vicinity of the mantle source of these basalts. The identification of HA basalts in the same region from where the Apollo 14 basalts originated would also extend the duration of aluminous volcanism in this region.

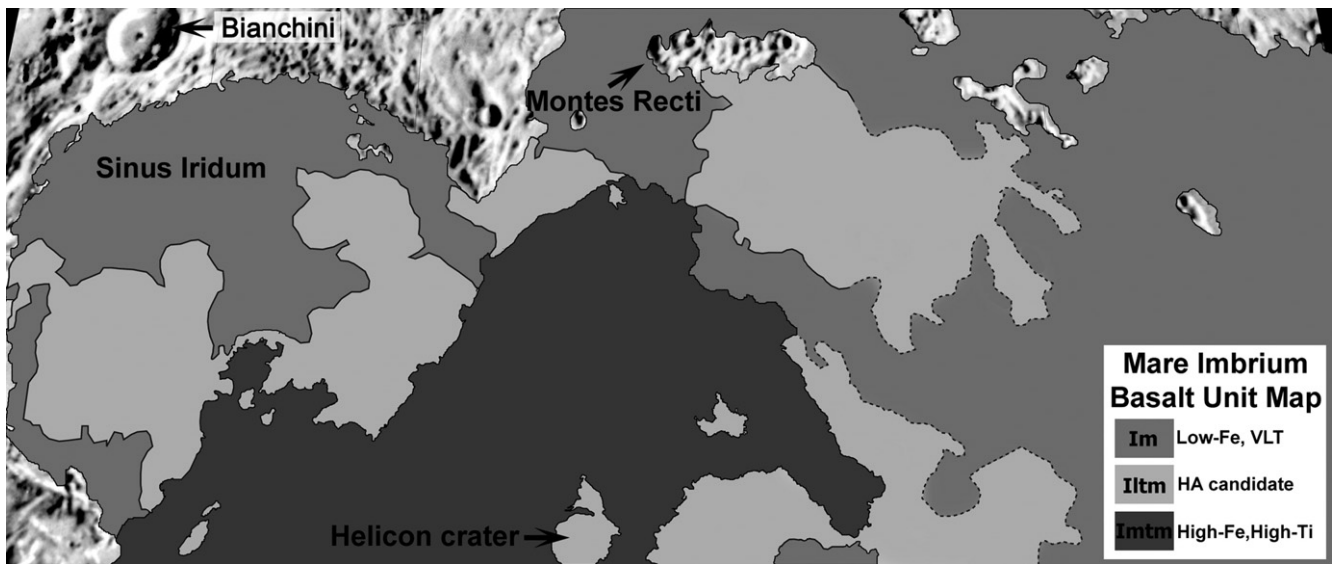


Fig. 8. Map of Northern Imbrium depicting major compositional mare units.

Fig. 8 is our map of the mare basalt compositional units identifiable with current remote sensing data. Units are delineated based on distinct compositional variations apparent from Clementine-derived FeO, TiO₂, and color ratio composite images (Fig. 9), as well as morphological interpretations from Lunar Orbiter photographs and the Clementine 750 nm band. Age variations from crater counting statistics of previous workers (Boyce and Dial, 1975; Hiesinger et al., 2000) are also factored in unit designations. As this region is located above 40° N, effects due to lighting geometry and the incidence angle of the camera (Jolliff, 1999; Kramer et al., 2008), especially on topographic features were exacerbated. These effects were taken into account when reviewing the data from small-crater rims and proximal ejecta used to characterize the basalt units.

3.2.1. Low-Fe, VLT unit: Im

At least two mare basalt units have been identified in the northern portion of Mare Imbrium by previous workers (e.g., Boyce, 1976; Pieters, 1978; Wilhelms, 1987; Hiesinger et al., 2000). Even a cursory look at Fig. 9 demonstrates the clear distinction of these two units: a low-Ti unit (red in Fig. 9b) and a higher-Ti unit (blue in Fig. 9b).

We divided the low-Ti portion of Mare Imbrium into two units based initially on the subtle difference in hues in the “red” mare, as can be seen in the color composite image (Fig. 9b). There are distinct patches that are more magenta than red. The magenta color indicates the blue channel (415/750 nm) of the color composite image contributes a slightly higher value than it does in the red regions.

Delineation of unit Im was ultimately the result of what remained after determining the boundaries of unit Iltm, so this is further discussed in the next section. We interpret unit Im to be the oldest of the three distinguished mare basalt units based on the apparent superposition of unit Iltm atop unit Im. Since our unit boundaries do not match closely enough with those of Hiesinger et al. (2000) we could not incorporate their crater counting statistics into a relative age distinction between units Iltm and Im. Small, immature impacts into unit Im (Table 7) indicate a unit composition of 14–15.5 wt% FeO and 0.5–1.5 wt% TiO₂, classifying it as a very low-Ti (VLT) mare basalt (Neal et al., 1988). Although Im has relatively low FeO, suggesting a high Al₂O₃, its TiO₂ abundance falls below our constraints for a HA basalt.

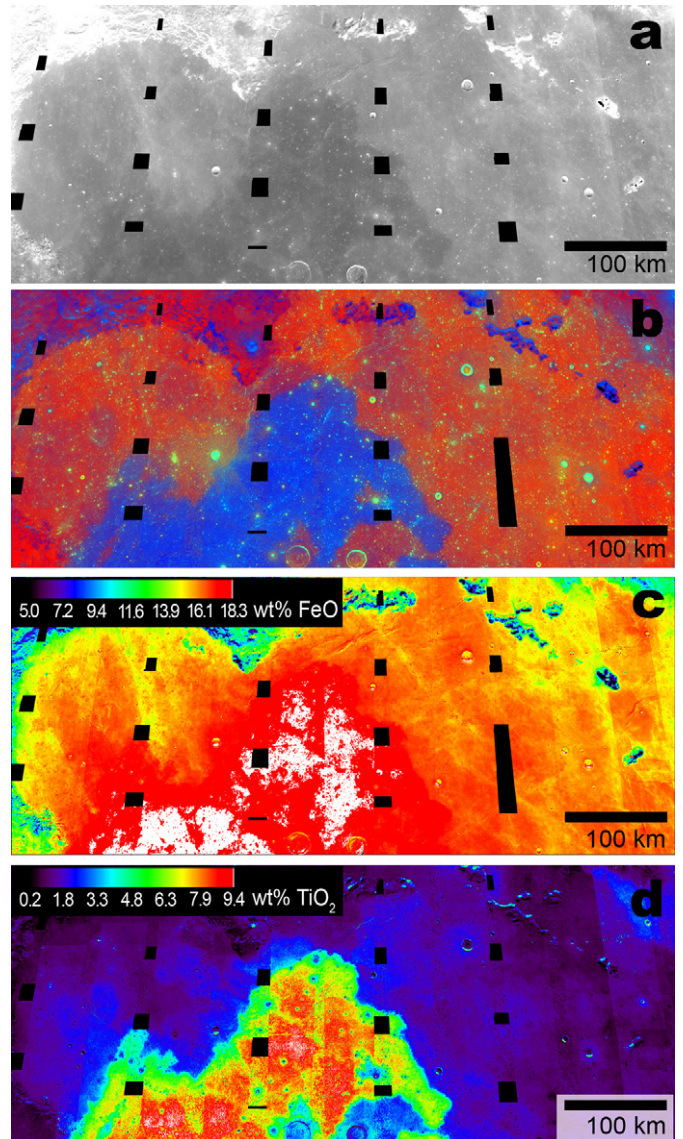


Fig. 9. Clementine imagery for northern Mare Imbrium. (a) 750 nm reflectance, (b) ratio, (c) FeO (Lucey et al., 2000b; Wilcox et al., 2005), (d) TiO₂ (Lucey et al., 2000b).

Table 7

Mean compositions and maturity of small craters in Northern Mare Imbrium's basalt unit Im

| FeO | TiO ₂ | OMAT | FeO | TiO ₂ | OMAT | FeO | TiO ₂ | OMAT |
|-------------------|------------------|--------|------|------------------|--------|------|------------------|--------|
| 0.4–1 km diameter | | | | | | | | |
| 14.2 | 0.3 | -0.696 | 14.7 | 0.5 | -0.835 | 16 | 1.3 | -0.853 |
| 12.9 | 0.2 | -0.703 | 16 | 0.6 | -0.837 | 16.6 | 1.4 | -0.854 |
| 15.3 | 0.4 | -0.745 | 16.3 | 0.9 | -0.837 | 16.8 | 1.1 | -0.855 |
| 15.2 | 0.4 | -0.768 | 15.1 | 0.7 | -0.837 | 15.8 | 0.8 | -0.856 |
| 12.4 | 0.3 | -0.768 | 14.1 | 0.5 | -0.837 | 15.4 | 1 | -0.857 |
| 13.2 | 0.3 | -0.769 | 16.3 | 0.6 | -0.837 | 16.5 | 0.9 | -0.857 |
| 16.8 | 0.7 | -0.778 | 15.3 | 0.9 | -0.838 | 15.4 | 0.6 | -0.857 |
| 15.3 | 0.9 | -0.784 | 14.8 | 0.4 | -0.838 | 17.3 | 1.7 | -0.858 |
| 16 | 0.7 | -0.789 | 14.8 | 0.7 | -0.838 | 14 | 0.8 | -0.858 |
| 16.3 | 0.8 | -0.79 | 14.9 | 0.8 | -0.838 | 15.5 | 0.9 | -0.858 |
| 17.5 | 0.9 | -0.792 | 16.1 | 1.5 | -0.838 | 15.5 | 0.4 | -0.858 |
| 16.6 | 1 | -0.8 | 15.5 | 0.9 | -0.838 | 16 | 1 | -0.859 |
| 16.8 | 1.1 | -0.8 | 14 | 0.9 | -0.839 | 14.9 | 0.6 | -0.86 |
| 16.2 | 0.8 | -0.8 | 16.1 | 1.7 | -0.84 | 16.2 | 1.2 | -0.861 |
| 16.7 | 0.8 | -0.805 | 14.5 | 0.7 | -0.841 | 15.3 | 0.6 | -0.861 |
| 12 | 0.4 | -0.808 | 15.2 | 0.6 | -0.841 | 17 | 2.1 | -0.862 |
| 14.5 | 1.6 | -0.808 | 16.9 | 1.3 | -0.842 | 14.1 | 0.7 | -0.862 |
| 15.7 | 0.5 | -0.81 | 15 | 0.6 | -0.843 | 16.7 | 1.5 | -0.863 |
| 16.2 | 1 | -0.813 | 15.6 | 0.8 | -0.843 | 15.8 | 1.1 | -0.864 |
| 15.7 | 0.6 | -0.813 | 16.3 | 1.1 | -0.843 | 16.6 | 0.9 | -0.865 |
| 14.6 | 0.4 | -0.815 | 15.8 | 1.7 | -0.843 | 14.6 | 0.9 | -0.865 |
| 14.4 | 0.4 | -0.82 | 16.2 | 0.9 | -0.843 | 15.4 | 1.4 | -0.865 |
| 15.3 | 0.5 | -0.821 | 14.2 | 0.6 | -0.843 | 17.4 | 1.4 | -0.866 |
| 14.8 | 0.5 | -0.822 | 16.6 | 1 | -0.844 | 17.2 | 1.5 | -0.866 |
| 14.4 | 0.4 | -0.824 | 15.9 | 0.6 | -0.844 | 15.9 | 1.2 | -0.866 |
| 15.3 | 0.8 | -0.825 | 16.1 | 0.8 | -0.845 | 14.4 | 0.6 | -0.867 |
| 16.1 | 0.8 | -0.825 | 17.3 | 1.4 | -0.845 | 15.6 | 0.8 | -0.869 |
| 15 | 1.1 | -0.826 | 17.3 | 1.2 | -0.845 | 16.4 | 1.8 | -0.871 |
| 16.1 | 1.4 | -0.829 | 14.7 | 1 | -0.845 | 14.8 | 0.8 | -0.871 |
| 17.8 | 1.6 | -0.829 | 16.7 | 1.2 | -0.846 | 17.3 | 2 | -0.876 |
| 16.9 | 0.9 | -0.829 | 15.8 | 0.8 | -0.846 | 15.6 | 1.2 | -0.879 |
| 15.9 | 0.6 | -0.829 | 14.8 | 1 | -0.847 | 15.7 | 0.8 | -0.879 |
| 15.6 | 1.3 | -0.83 | 16.4 | 1.1 | -0.847 | 16.1 | 1.1 | -0.88 |
| 15.3 | 0.8 | -0.831 | 16.8 | 1.4 | -0.848 | 16 | 1.5 | -0.883 |
| 14.9 | 0.9 | -0.832 | 15.2 | 0.8 | -0.848 | 17.8 | 2.7 | -0.885 |
| 16 | 0.9 | -0.832 | 15.8 | 0.8 | -0.848 | 15.7 | 1.1 | -0.885 |
| 16.7 | 1 | -0.833 | 14.6 | 0.7 | -0.849 | 14.2 | 0.8 | -0.886 |
| 15.5 | 0.8 | -0.833 | 17.3 | 1.4 | -0.851 | 15.1 | 0.7 | -0.886 |
| 15.8 | 0.6 | -0.833 | 15.1 | 0.9 | -0.851 | 15.7 | 0.9 | -0.888 |
| 14.8 | 1.3 | -0.834 | 16.1 | 0.8 | -0.851 | 16.7 | 1.3 | -0.89 |
| 15.2 | 0.8 | -0.835 | 17.5 | 1.2 | -0.852 | 16.2 | 1.4 | -0.891 |
| 17.2 | 1.1 | -0.835 | 16.1 | 1.2 | -0.852 | 15.5 | 1 | -0.891 |
| 16.9 | 0.9 | -0.835 | 16.8 | 1.2 | -0.852 | 16.2 | 2.3 | -0.899 |
| 1–2 km diameter | | | | | | | | |
| 17.6 | 1.5 | -0.688 | 14.7 | 0.7 | -0.833 | 16.2 | 1 | -0.866 |
| 16.3 | 0.8 | -0.787 | 13.9 | 0.5 | -0.837 | 16 | 2.2 | -0.866 |
| 16.1 | 0.7 | -0.8 | 14.6 | 0.4 | -0.837 | 17.9 | 2.1 | -0.868 |
| 17.2 | 1.1 | -0.806 | 13.7 | 1 | -0.837 | 17.4 | 2.1 | -0.868 |
| 13.7 | 0.8 | -0.81 | 14.9 | 0.4 | -0.84 | 17.2 | 1.5 | -0.868 |
| 14.8 | 0.7 | -0.813 | 16.3 | 1 | -0.845 | 14.6 | 0.9 | -0.872 |
| 16.7 | 1.2 | -0.813 | 14.9 | 0.8 | -0.846 | 15.5 | 0.6 | -0.873 |
| 14.3 | 0.8 | -0.814 | 16.1 | 1.1 | -0.846 | 15.7 | 1 | -0.874 |
| 14.6 | 0.5 | -0.815 | 16.5 | 1.7 | -0.847 | 14.1 | 0.9 | -0.874 |
| 13.9 | 0.4 | -0.819 | 13.4 | 0.8 | -0.852 | 14.3 | 0.6 | -0.877 |
| 14.2 | 0.6 | -0.821 | 13.9 | 0.8 | -0.854 | 16.1 | 1.2 | -0.878 |
| 15.4 | 0.8 | -0.826 | 16.1 | 2.3 | -0.856 | 15.9 | 0.7 | -0.89 |
| 14.7 | 0.8 | -0.828 | 15.4 | 1 | -0.859 | 13.6 | 0.6 | -0.892 |
| 15.4 | 0.9 | -0.831 | 15.9 | 1.2 | -0.861 | 14.4 | 0.8 | -0.892 |
| 17.1 | 1.4 | -0.831 | 15.2 | 1.1 | -0.864 | 15 | 1 | -0.895 |
| 2–3 km diameter | | | | | | | | |
| 15 | 0.5 | -0.8 | 14.1 | 0.8 | -0.82 | 14.3 | 1.2 | -0.833 |
| 14.6 | 1 | -0.801 | | | | | | |
| 3–4 km diameter | | | | | | | | |
| 15.8 | 1.1 | -0.826 | 15.2 | 1.9 | -0.848 | 15.7 | 2 | -0.867 |
| 14.9 | 1.3 | -0.847 | 14.1 | 0.7 | -0.852 | | | |

3.2.2. Mid-Fe, low-Ti unit: Iltm

We initially divided the low-Ti “super-unit” into units Im and Iltm based on subtle color differences of the mare surface in a color composite image (Fig. 9b) and TiO₂ image (Fig. 9d). Once thus divided, we could adjust or support these unit delineations from

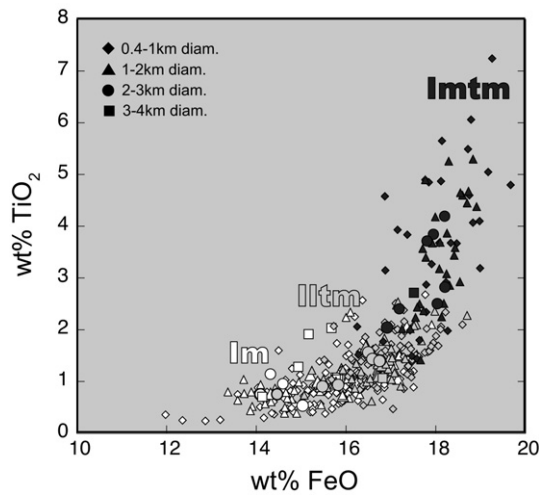


Fig. 10. FeO vs TiO₂ for rims and proximal ejecta of small impacts into northern Mare Imbrium.

the analysis of compositions and spectra derived from the ejecta of small impact into each unit. A plot of the FeO and TiO₂ abundances (Fig. 10, Table 8) revealed by small impacts into both units shows a fairly distinct separation of ejecta compositions that correlates with the division of the units based on their color differences in Fig. 9b. Ejecta compositions from the differentiated units do not overlap in Northern Mare Imbrium even to the extent seen in other ROIs (Kramer et al., 2008), including Mare Fecunditatis (Fig. 7).

We then compared the spectra from craters into both the magenta and red regions and found a slight difference. Although spectral shape is generally the same, suggesting a similar mineralogy, the magenta regions have a slightly subdued Fe absorption and an overall flattening of the spectra compared with the redder regions (Fig. 11). This is consistent with the increased contribution from the blue channel in Fig. 9b, which is interpreted as reflecting a relatively higher amount of TiO₂.

We interpret the composition of unit Iltm to be best represented by the densest clustering of points representing small impact ejecta compositions, as depicted in Fig. 10: 16–17.5 wt% FeO and 1–2 wt% TiO₂. These abundances fall within the constraints for a HA basalt, and are consistent with the low-Ti composition of the Apollo 14 HA basalts.

Northern Mare Imbrium was also studied by Hiesinger et al. (2000) as part of an comprehensive analysis of nearside mare basalts. This group delineated their spectral units based on a color ratio composite of Galileo Earth/Moon Encounter imaging data, which has different wavelengths, and therefore different band ratios than Clementine. They identified five different mare basalt units, based on subtle differences in spectral properties of the mare surface, in the same boundary of this ROI, one being the higher-Ti unit. They also found five different ages for each unit designation based on crater-size frequency distribution measurements. The conclusions from our analysis of northern Mare Imbrium compare fairly well with those of Hiesinger et al. (2000), despite our different methods and data sets. The focus of the work by Hiesinger et al. (2000) on the mare surface compared with our focus on the sub-regolith basalt composition revealed by small impacts is likely what led to our divergent conclusions.

3.2.3. High-Fe, mid-Ti unit: Imtm

Unit Imtm is clearly distinguishable as a discrete unit in northern Mare Imbrium. Our independent delineation of its boundaries marks the same area as identified by Pieters (1978), Wilhelms (1987), and Hiesinger et al. (2000), and because of this agreement, we can conclude that Imtm is the youngest of the three mare

Table 8

Mean compositions and maturity of small craters in Northern Mare Imbrium's basalt unit Iltm

| FeO | TiO ₂ | OMAT | FeO | TiO ₂ | OMAT | FeO | TiO ₂ | OMAT |
|-------------------|------------------|--------|------|------------------|--------|------|------------------|--------|
| 0.4–1 km diameter | | | | | | | | |
| 15.7 | 1 | −0.742 | 16.6 | 1 | −0.83 | 16.8 | 2 | −0.854 |
| 17.3 | 0.9 | −0.762 | 16.9 | 1.6 | −0.831 | 17.5 | 1.1 | −0.86 |
| 16.4 | 0.5 | −0.774 | 17.9 | 1.6 | −0.832 | 16.4 | 0.9 | −0.861 |
| 17.4 | 1.3 | −0.776 | 16.8 | 1.6 | −0.832 | 15.7 | 2.1 | −0.862 |
| 17.4 | 1.3 | −0.785 | 17.8 | 1.6 | −0.833 | 16.7 | 1.4 | −0.863 |
| 16.4 | 0.9 | −0.787 | 16.3 | 1.1 | −0.833 | 17.2 | 1.9 | −0.863 |
| 17.4 | 1.2 | −0.797 | 16.4 | 1.4 | −0.833 | 17.8 | 2 | −0.864 |
| 17.4 | 1.1 | −0.799 | 16.7 | 1.4 | −0.833 | 15.6 | 1 | −0.865 |
| 16.3 | 1.6 | −0.799 | 18.1 | 2.1 | −0.837 | 17.6 | 1.5 | −0.867 |
| 16.3 | 0.9 | −0.799 | 16.6 | 1.4 | −0.838 | 17.3 | 2.2 | −0.867 |
| 16.3 | 0.8 | −0.8 | 18.6 | 2.1 | −0.84 | 17.6 | 1.5 | −0.869 |
| 16.8 | 1.1 | −0.8 | 18.1 | 2 | −0.841 | 18 | 1.8 | −0.87 |
| 16.6 | 1 | −0.807 | 16.5 | 1.4 | −0.841 | 18.2 | 2.3 | −0.87 |
| 16.6 | 0.9 | −0.808 | 17.4 | 2 | −0.842 | 16.3 | 1.4 | −0.87 |
| 17.4 | 1.1 | −0.815 | 16.4 | 1 | −0.843 | 16.8 | 1.4 | −0.874 |
| 16.8 | 1.1 | −0.815 | 15.5 | 1.4 | −0.843 | 16.9 | 1.6 | −0.875 |
| 16.6 | 1 | −0.815 | 17.5 | 1.4 | −0.844 | 16.4 | 1.9 | −0.876 |
| 16.1 | 1.2 | −0.816 | 16.5 | 1.3 | −0.845 | 17.2 | 1.7 | −0.877 |
| 16.3 | 1 | −0.818 | 16.7 | 1.7 | −0.847 | 17 | 1.5 | −0.877 |
| 17.5 | 1.4 | −0.819 | 17.2 | 2 | −0.848 | 16.1 | 1.4 | −0.879 |
| 18.1 | 1.7 | −0.82 | 17.9 | 1.7 | −0.849 | 16.6 | 1.6 | −0.88 |
| 17.1 | 0.5 | −0.824 | 15.9 | 1.2 | −0.849 | 17.4 | 1.7 | −0.887 |
| 16.7 | 0.9 | −0.824 | 17.1 | 2 | −0.849 | 16.9 | 2.1 | −0.889 |
| 16.9 | 1.2 | −0.828 | 18 | 1.9 | −0.852 | 17.1 | 2.5 | −0.889 |
| 17.3 | 1.5 | −0.829 | 17.9 | 1.6 | −0.854 | 17 | 1.7 | −0.89 |
| 1–2 km diameter | | | | | | | | |
| 18.7 | 2.3 | −0.668 | 16.2 | 1.4 | −0.835 | 17.3 | 1.4 | −0.859 |
| 15.1 | 0.7 | −0.697 | 16.9 | 1.8 | −0.835 | 16.3 | 1.2 | −0.862 |
| 16.9 | 1.2 | −0.777 | 17.2 | 2.5 | −0.836 | 18 | 2.4 | −0.865 |
| 16.6 | 0.6 | −0.795 | 17.5 | 2.1 | −0.84 | 15.5 | 1 | −0.868 |
| 15.6 | 0.9 | −0.796 | 17.1 | 1.2 | −0.843 | 17 | 1.4 | −0.871 |
| 17 | 1 | −0.799 | 16.1 | 1.1 | −0.844 | 17.5 | 2.1 | −0.871 |
| 16.2 | 0.9 | −0.801 | 17.1 | 1.2 | −0.849 | 15.2 | 1.2 | −0.873 |
| 16.7 | 1.4 | −0.808 | 17.7 | 1.8 | −0.849 | 16.4 | 1.7 | −0.875 |
| 15.8 | 1 | −0.811 | 17 | 1.5 | −0.852 | 16.7 | 1.2 | −0.877 |
| 15.9 | 1.2 | −0.822 | 16.9 | 1.3 | −0.855 | 16.5 | 1 | −0.879 |
| 17.2 | 0.9 | −0.829 | 17 | 1.6 | −0.856 | 16.7 | 1.1 | −0.899 |
| 16.5 | 1.1 | −0.832 | 16.8 | 1.3 | −0.856 | | | |
| 2–3 km diameter | | | | | | | | |
| 16.7 | 1.4 | −0.778 | 16.6 | 1.4 | −0.818 | 16.5 | 1.6 | −0.845 |
| 14.5 | 0.8 | −0.797 | 15.8 | 0.9 | −0.835 | 16.8 | 1.4 | −0.852 |
| 3–4 km diameter | | | | | | | | |
| 16.8 | 1.1 | −0.885 | | | | | | |

basalt units in northern Mare Imbrium. Unit Iltm is spectrally darker (Fig. 9a), has a high 450/750 nm value (depicted in the blue channel of Fig. 9b), and has an FeO and TiO₂ abundance that exceeds the range of all sampled HA basalts (Figs. 9c, 9d). Basalt spectra from the rims and proximal ejecta of small craters (Fig. 11) in this unit have a lower reflectance over all wavelengths and display a very subdued Fe absorption compared with the ejecta from craters into Im and Iltm.

Small-crater ejecta compositions range from 16.5–19.5 wt% FeO and 2–7 wt% TiO₂ (Table 9). The narrow range in FeO, and wide range in TiO₂ suggests regolith deposited atop the analyzed crater ejecta have been contaminated by the lower-Fe, and significantly lower-Ti units to the north. Some of the craters may have penetrated through the unit, and sampled an underlying low-Ti basalt, perhaps the underlying extent of unit Im or Iltm. Since unit Iltm has the highest TiO₂ and FeO abundances in the ROI, there is no other source for a high-Ti contribution to the regolith. We therefore conclude that the highest TiO₂ abundances measured in the ejecta of small crater into Imtm best represent the composition of the unit. Imtm has an FeO abundance between 18.5 and 20 wt% FeO and TiO₂ abundance between 5.5 and 7 wt% TiO₂.

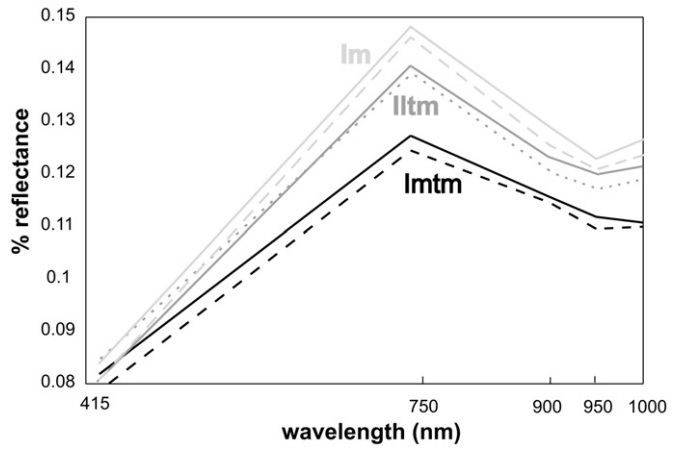


Fig. 11. Spectra from Clementine UV-VIS-IR of rims and proximal ejecta of small impacts into northern Mare Imbrium.

Table 9

Mean compositions and maturity of small craters in Northern Mare Imbrium's basalt unit Iltm

| FeO | TiO ₂ | OMAT | FeO | TiO ₂ | OMAT | FeO | TiO ₂ | OMAT |
|-------------------|------------------|--------|------|------------------|--------|------|------------------|--------|
| 0.4–1 km diameter | | | | | | | | |
| 17.6 | 1.4 | −0.713 | 17.4 | 3.8 | −0.839 | 18.7 | 5.5 | −0.865 |
| 16.3 | 2.1 | −0.76 | 18.1 | 3.7 | −0.842 | 18.1 | 5.7 | −0.869 |
| 16.8 | 1.8 | −0.788 | 17.2 | 3.9 | −0.843 | 17.9 | 4.9 | −0.87 |
| 12 | 4.6 | −0.797 | 19 | 3.2 | −0.844 | 17.9 | 3.3 | −0.87 |
| 18 | 2.5 | −0.813 | 16.3 | 1.5 | −0.844 | 17.8 | 4.9 | −0.872 |
| 17.8 | 2.3 | −0.814 | 17.6 | 1.8 | −0.847 | 19.2 | 5.1 | −0.875 |
| 16.9 | 3.2 | −0.82 | 18.3 | 2 | −0.851 | 18.8 | 6.1 | −0.878 |
| 18.2 | 2.9 | −0.834 | 19.3 | 7.2 | −0.851 | 19 | 4.1 | −0.882 |
| 17.8 | 2.9 | −0.836 | 18.8 | 4.1 | −0.857 | 18.8 | 4.6 | −0.892 |
| 17.5 | 1.5 | −0.837 | 18.5 | 3.7 | −0.859 | 19.7 | 4.8 | −0.893 |
| 18.1 | 4.9 | −0.838 | 18.3 | 3.7 | −0.861 | | | |
| 1–2 km diameter | | | | | | | | |
| 17.7 | 1.4 | −0.801 | 18.4 | 3.4 | −0.846 | 18.7 | 4.5 | −0.879 |
| 17.6 | 2.2 | −0.808 | 18.2 | 3.1 | −0.851 | 17.7 | 3.6 | −0.879 |
| 17.3 | 2 | −0.815 | 18 | 4.2 | −0.856 | 17.8 | 3.4 | −0.881 |
| 17.7 | 2.4 | −0.82 | 18.1 | 3.7 | −0.861 | 18.3 | 3.9 | −0.882 |
| 17.9 | 3.7 | −0.823 | 17.4 | 2 | −0.864 | 18.7 | 4.7 | −0.886 |
| 17.6 | 2.4 | −0.829 | 18.1 | 2.3 | −0.865 | 18.6 | 4.7 | −0.89 |
| 17.6 | 2.5 | −0.829 | 18.3 | 5.3 | −0.869 | 18.8 | 5.3 | −0.897 |
| 18.2 | 2.5 | −0.833 | 18.4 | 3.6 | −0.87 | 18.3 | 2.9 | −0.9 |
| 18.1 | 3.2 | −0.842 | 17.8 | 4.9 | −0.871 | | | |
| 2–3 km diameter | | | | | | | | |
| 18.2 | 2.8 | −0.812 | 17.2 | 2.4 | −0.854 | 17.9 | 3.9 | −0.89 |
| 18 | 2.5 | −0.841 | 17.8 | 3.7 | −0.862 | 18.2 | 4.2 | −0.893 |
| 16.9 | 2.1 | −0.849 | | | | | | |
| 3–4 km diameter | | | | | | | | |
| 17.5 | 2.7 | −0.828 | | | | | | |

4. Summary and conclusions

Sample geochemistry of mare basalts indicates that they derived from sources composed of late-stage cumulates of the Lunar Magma Ocean (LMO) (Taylor and Jakes, 1974; Snyder et al., 1992; Shearer and Papike, 1999). The aluminous nature of both the Apollo 14 and Luna 16 basalts is manifest in the fact that they contain proportionally greater modal plagioclase relative to mare basalts from other sample return sites (e.g., Albee et al., 1972; Papike et al., 1974; Papike and Vaniman, 1978; Neal and Taylor, 1992). Therefore, their existence alludes to the depth and extent of source melting, differentiation within the lunar mantle, and to the efficiency of plagioclase separation from earlier forming, mafic cumulates during crystallization of the Lunar Magma Ocean (LMO). Source modeling of these basalts indicates a significant proportion of plagioclase remained in their source regions (Neal and

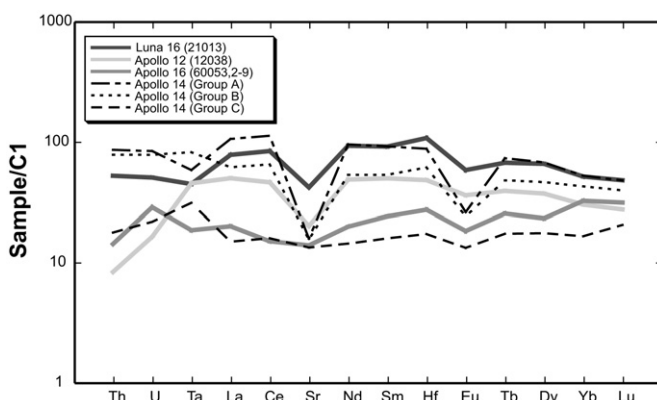


Fig. 12. Chondrite-normalized trace element profile of HA mare basalts. X-axis is trace element with decreasing incompatibility from left to right. Line pattern reflects parental compositions and mineral fractionation in the magma. Apollo 14 HA basalts break into 3 groups (A, B, C) based on age and composition (see Neal and Kramer, 2006). Groups A, B, and C depicted here represent an average composition for each group. Apollo 14 data from Neal and Kramer (2006). Luna 16 data are an average of compositions for sample 21003 from Ma et al. (1979). Apollo 12 sample 12038 data from Brunfelt et al. (1972). Apollo 16 data from Zeigler et al. (2006).

Kramer, 2006). Luna 16 HA basalts exhibit a slightly bow-shaped chondrite-normalized REE profile, whereas most Apollo 14 basalts are LREE enriched to varying degrees (Fig. 12) (Taylor et al., 1991; Neal and Kramer, 2006). This LREE enrichment may be due to the Apollo 14 HA basalts' origin in the PKT, and certainly reflects the heterogeneity of the lunar mantle.

The constraints used to search the lunar surface for HA basalts located two regions that are the best candidates from where sampled HA basalts originally erupted—Mare Fecunditatis for Luna 16 samples and northern Mare Imbrium for Apollo 14 samples. There are two HA basalt units identified in Mare Fecunditatis that are consistent with sampled HA basalts, although only unit Iltm is a compositional match for the Luna 16 HA samples. Radiometric ages of Luna 16 sampled HA basalts are also consistent with the relative surface age of northern Mare Fecunditatis (Wilhelms, 1987), providing further evidence that this unit may be parental to the sampled basalts. Northern Mare Imbrium also reveals two units that are within the compositional constraints of a HA basalt when accounting for uncertainty in the FeO and TiO₂ data. However, one unit (Iltm) is the best match to the sampled Apollo 14 HA basalts.

The ROLs analyzed in northern Mare Imbrium cannot be directly related to the Apollo 14 samples. Most Apollo 14 HA basalts occurred as clasts in impact melt breccias collected from the Fra Mauro Formation, a region formed of ejecta from the Imbrium impact (Wilhelms, 1987). Radiometrically derived ages for the Apollo 14 HA basalts show them all to have erupted prior to formation of the Imbrium basin. For these reasons, Apollo 14 HA basalts are interpreted as having originated at or near Imbrium basin prior to its formation. Therefore, we could not find the true parental basalt units for the Apollo 14 HA samples, as they have surely been destroyed and/or covered by subsequent mare basalt flows. However, where mantle sources for the pre-Imbrian HA basalts once erupted, they might have erupted again. The three sources for the Apollo 14 HA basalts melted and erupted at least three times over a span of 400 million years (Papanastassiou and Wasserburg, 1971; Shervais et al., 1985; Dasch et al., 1987). The last eruption occurred less than 100 million years before the Imbrium impact. Energy associated with the Imbrian event may even have facilitated melting of the source and/or subsequent eruption. Basin formation provided an easier conduit, in the form of a fractured and thinner crust, and a vast topographic depression into which the erupted basalts could coalesce. A post-Imbrian HA eruption into the Imbrium basin is not an unlikely event.

Our initial search for HA basalts (Fig. 1) identified their presence in several locations across the lunar surface. By establishing the immanence of HA basalts on the Moon we can demonstrate that plagioclase retention was not limited to a few isolated regions, but may have been a Moon-wide phenomenon. A quantitative model of the LMO would benefit from knowing their occurrence.

The biggest obstacle in analyzing the lunar surface is the paucity of high spatial and spectral resolution of the Moon from which to derive robust compositional information. The current data sets provide limited information, and suffer from low precision in the information that is available. For discerning HA basalts in particular, FeO and TiO₂ surface compositions can mimic the composition of a mixture of high-Fe/low-Al₂O₃ mare basalts and low-FeO/high-Al₂O₃ feldspathic highland materials. The likelihood that some or many of the HA basalts are old and thus buried by basin ejecta or younger basalt flows further exacerbates the problem. However, we have demonstrated that an assessment of the geology and actual distribution of materials with distinctive compositions at the resolution of Clementine data can be used to evaluate whether mixing produced the composition or whether a bona-fide high-Al basalt might in fact lie beneath the regolith.

The described method of small impact ejecta analysis is a valuable tool for evaluating the sub-regolith bedrock lithologies. We are currently studying details of crater dynamics to develop a procedure, and testing aspects of its strengths with actual and theoretical data. Current and future lunar missions, such as Lunar Reconnaissance Orbiter and Chandrayaan-1, will provide much stronger data sets with which to better detect HA basalts, locate lithologies of interest, and understand the lunar environment in preparation for our manned return to the Moon.

Acknowledgments

This research was partially supported by NASA Cosmochemistry Grant NAG5-12982 (C.R.N.) and NASA Planetary Geology and Geophysics grant (NNG05GI38G) (B.L.J.). The first author wished to express thanks to scientists and staff at the Lunar and Planetary Institute for their assistance with this research. The first author also wishes to thank Jean-Philippe Combe for his review of this paper, as well as the insightful comments and suggestions from the reviewers assigned by Icarus.

References

- Albee, A.L., Chodos, A.A., Gancarz, A.J., Haines, E.L., Papanastassiou, D.A., Ray, L., Tera, F., Wasserburg, G.J., Wen, T., 1972. Mineralogy, petrology, and chemistry of Luna 16 sample b-1. *Lunar Sci. III*, 10–11.
- Boyce, J.M., 1976. Ages of flow units in the lunar nearside maria based on Lunar Orbiter IV photographs. *Proc. Lunar Sci. Conf.* 7, 2717–2728.
- Boyce, J.M., Dial, A.L., 1975. Relative ages of flow units in Mare Imbrium and Sinus Iridum. *Proc. Lunar Sci. Conf.* 6, 2585–2595.
- Brunfelt, A.O., Heier, K.S., Nilssen, B., Sundvoll, B., Steinnes, E., 1972. Distribution of elements between different phases of Apollo 14 rocks and soils. *Proc. Lunar Sci. Conf.* 3, 1133–1147.
- Cadogan, P.H., Turner, G., 1977. ⁴⁰Ar–³⁹Ar dating of Luna 16 and Luna 20 samples. *Philos. Trans. R. Soc. London A* 284, 167–177.
- Cohen, B.A., Snyder, G.A., Hall, C.M., Taylor, L.A., Nazarov, M.A., 2001. Argon-40–argon-39 chronology and petrogenesis along the eastern limb of the Moon from Luna 16, 20, and 24 samples. *Meteor. Planet. Sci.* 36, 1345–1366.
- Dasch, E.J., Shih, C.Y., Bansal, B.M., Weismann, H., Nyquist, L.E., 1987. Isotopic analysis of basaltic fragments from lunar breccia 14321: Chronology and petrogenesis of pre-Imbrium mare volcanism. *Geochim. Cosmochim. Acta* 51, 3241–3254.
- DeHon, R.A., 1975. Mare Fecunditatis: Basin configuration. In: Conference on the Origins of Mare Basalts and Their Implications for Lunar Evolution. *Lunar Planet. Inst.*, Houston, TX, pp. 32–34.
- Dickinson, T., Taylor, G.J., Keil, K., Schmitt, R.A., Hughes, S.S., Smith, M.R., 1985. Apollo 14 aluminous mare basalts and their possible relationship to KREEP. *J. Geophys. Res.* 90, C365–C375.
- Duncan, A.R., McKay, S.M., Stoeser, J.W., Lindstrom, M.M., Lindstrom, D.J., Fruchter, J.S., Goles, G.G., 1975. Lunar polymict breccia 14321: A compositional study of its principle components. *Geochim. Cosmochim. Acta* 39, 247–260.

- Ehmann, W.D., Gillum, D.E., Morgan, J.W., 1972. Oxygen and bulk elemental composition studies of Apollo 14 and other lunar rocks and soils. *Geochim. Cosmochim. Acta* 2, 1149–1160.
- El Goresy, A., Taylor, L.A., Ramdohr, P., 1972. Fra Mauro crystalline rocks: Mineralogy, geochemistry, and subsolidus reduction of the opaque minerals. *Geochim. Cosmochim. Acta* 1 (Suppl. 3), 333–349.
- Eliason, E.M., 1997. Production of digital image models using the ISIS system. *Lunar Planet. Sci. XXVIII*, 331–332. Abstract.
- Feldman, W.C., Barracough, B.L., Fuller, K.R., Lawrence, D.J., Maurice, S., Miller, M.C., Prettyman, T.H., Binder, A.B., 1999. The Lunar Prospector gamma-ray and neutron spectrometers. *Nucl. Instrum. Methods Phys. Res., Sect. A* 422, 562–566.
- Fernandes, V.A., Burgess, R., Turner, G., 2000. Laser argon-40-argon-39 age studies of Dar al Gani 262 meteorite. *Meteor. Planet. Sci.* 35, 1355–1364.
- Finnila, A.B., Hess, P.C., Rutherford, M.J., 1994. Assimilation by lunar mare basalts: Melting of crustal material and dissolution of anorthosite. *J. Geophys. Res.* 99, 14677–14690.
- Grieve, R.A.F., McKay, G.A., Weill, D.F., 1972. Microprobe studies of three Luna 16 basalt fragments. *Earth Planet. Sci. Lett.* 13, 233–242.
- Grieve, R.A.F., McKay, G.A., Smith, H.D., Weill, D.F., 1975. Lunar polymict breccia 14321: A petrographic study. *Geochim. Cosmochim. Acta* 39, 229–246.
- Hagerty, J.J., Shearer, C.K., Papike, J.J., 2005. Trace element characteristics of the Apollo 14 high-alumina basalts: Implications for early magmatism on the Moon. *Geochim. Cosmochim. Acta* 69, 5831–5845.
- Hawke, B.R., Gillis, J.J., Giguere, T.A., Blewett, D.T., Lawrence, D.J., Lucey, P.G., Peterson, C.A., Smith, G.A., Spudis, P.D., Taylor, G.J., 2005a. The earliest mare basalts. *Lunar Planet. Sci. XXXVI*, 1642. Abstract.
- Hawke, B.R., Gillis, J.J., Giguere, T.A., Blewett, D.T., Lawrence, D.J., Lucey, P.G., Smith, G.A., Spudis, P.D., Taylor, G.J., 2005b. Remote sensing and geologic studies of the Balmer-Kapteyn region of the Moon. *J. Geophys. Res.* 110, doi:10.1029/2004JE002383.
- Heimke, P.A., Haskin, L.A., 1972. Rare earths and other trace elements in Luna 16 soil. *Earth Planet. Sci. Lett.* 13, 441–443.
- Hiesinger, H., Jaumann, R., Neukum, G., Head, J.W., 2000. Ages of mare basalts on the lunar nearside. *J. Geophys. Res.* 105 (E12), 29239–29275.
- Hubbard, N.J., Gast, P.W., Rhodes, J.M., Bansal, B.M., Wiesmann, H., 1972a. Nonmare basalts: Part II. *Proc. Lunar Sci. Conf.* 3, 1161–1179.
- Hubbard, N.J., Gast, P.W., Rhodes, J.M., Bansal, B.M., Wiesmann, H., 1972b. Nonmare basalts: Part II. *Geochim. Cosmochim. Acta* 2, 1161–1179.
- Hughes, S.S., Neal, C.R., Taylor, L.A., 1990. Petrogenesis of Apollo 14 high alumina (HA) parental basaltic magma. *Lunar Planet. Sci. XXI*, 540–541. Abstract.
- Huneke, J.C., Podosek, F.A., Wasserburg, G.J., 1972. Gas retention and cosmic-ray exposure ages of a basalt fragment from Mare Fecunditatis. *Earth Planet. Sci. Lett.* 13, 375–383.
- Jakes, P., Warner, J., Ridley, W.I., Reid, A.M., Harmon, R.S., Brett, R., Brown, R.W., 1972. Petrology of a portion of the Mare Fecunditatis regolith. *Earth Planet. Sci. Lett.* 13, 257–271.
- Jolliff, B.L., 1999. Clementine UVVIS multispectral data and the Apollo 17 landing site: What can we tell and how well? *J. Geophys. Res.* 104 (E6), 14123–14148.
- Kramer, G.Y., Neal, C.R., Jolliff, B.L., 2008. Distinguishing high alumina mare basalts using Clementine UVVIS and Lunar Prospector GRS data: Mare Moscoviense and Mare Nectaris. *J. Geophys. Res.* 113 (E1), doi:10.1029/2006JE002860.
- Kurat, G., Kracher, A., Keil, K., Warner, R., Prinz, M., 1976. Composition and origin of Luna 16 aluminous mare basalts. *Proc. Lunar Sci. Conf.* 7, 1301–1321.
- Lindstrom, M.M., Duncan, A.R., Fruchter, J.S., McKay, S.M., Stoeser, J.W., Goles, G.G., Lindstrom, D.J., 1972. Compositional characteristics of some Apollo 14 clastic materials. *Geochim. Cosmochim. Acta* 2, 1201–1214.
- Longhi, J., Walker, D., Hays, J., 1972. Petrography and crystallization history of basalts 14310 and 14072. *Proc. Lunar Sci. Conf.* 3, 131–139.
- Lucey, P.G., Blewett, D.T., Hawke, B.R., 2000a. Imaging of lunar surface maturity. *J. Geophys. Res.* 105 (E8), 20377–20386.
- Lucey, P.G., Blewett, D.T., Hawke, B.R., 2000b. Lunar iron and titanium abundance algorithms based on final processing of Clementine ultraviolet-visible images. *J. Geophys. Res.* 105 (E8), 20297–20305.
- Ma, M.S., Schmitt, R.A., Nielsen, R.L., Taylor, G.J., Warner, R.D., Keil, K., 1979. Petrogenesis of Luna 16 aluminous mare basalts. *Geophys. Res. Lett.* 6, 909–912.
- McCord, T.B., Adams, J.B., 1973. Progress in remote optical analysis of lunar surface composition. *Moon* 7, 453–474.
- Melosh, H.J., 1989. Impact Cratering: A Geologic Process. Oxford Univ. Press, New York, NY.
- Neal, C.R., 2001. Interior of the Moon: The presence of garnet in the primitive deep lunar mantle. *J. Geophys. Res.* 106, 27865–27885.
- Neal, C.R., 2006. Mare basalt database. Supplemental Material to New Views of the Moon. URL: <http://www.minsocam.org>.
- Neal, C.R., Kramer, G.Y., 2006. The petrogenesis of the Apollo 14 high-Al mare basalts. *Am. Mineral.* 91, 1521–1535.
- Neal, C.R., Taylor, L.A., 1989. Metasomatic products of the lunar magma ocean: The role of KREEP dissemination. *Geochim. Cosmochim. Acta* 53, 529–541.
- Neal, C.R., Taylor, L.A., 1992. Petrogenesis of mare basalts: A record of lunar volcanism. *Geochim. Cosmochim. Acta* 56, 2177–2211.
- Neal, C.R., Taylor, L.A., Lindstrom, M.M., 1988. Apollo 14 mare basalt petrogenesis: Assimilation of KREEP-like components by a fractionating magmas. *Proc. Lunar Sci. Conf.* 18, 139–153.
- Neal, C.R., Taylor, L.A., Patchen, A.D., 1989. High alumina (HA) and very high potassium (VHK) basalt clasts from Apollo 14 breccias, part 1: Mineralogy and petrology: Evidence of crystallization from evolving magmas. *Proc. Lunar Sci. Conf.* 19, 137–145.
- Nyquist, L.E., Shih, C.Y., 1992. The isotopic record of lunar volcanism. *Geochim. Cosmochim. Acta* 56, 2213–2234.
- Nyquist, L.E., Wooden, J.L., Shih, C.Y., Wiesmann, H., Bansal, B.M., 1981. Isotopic and REE studies of lunar basalt 12038: Implications for petrogenesis of aluminous basalts. *Earth Planet. Sci. Lett.* 55, 335–355.
- Papanastassiou, D.A., Wasserburg, G.A., 1971. Rb-Sr ages of the igneous rocks from the Apollo 14 mission and the age of the Fra Mauro formation. *Earth Planet. Sci. Lett.* 12, 36–48.
- Papike, J.J., Vaniman, D.T., 1978. The lunar mare basalt suite. *Geophys. Res. Lett.* 5 (6), 433–436.
- Papike, J.J., Bence, A.E., Lindsley, D.H., 1974. Mare basalts from the Taurus-Littrow region of the Moon. *Proc. Lunar Sci. Conf.* 5, 471–504.
- Pieters, C.M., 1978. Mare basalt types on the front side of the Moon: A summary of spectral reflectance data. *Proc. Lunar Sci. Conf.* 9, 2825–2849.
- Prettyman, T.H., Feldman, W.C., Lawrence, D.J., McKinney, G.W., Binder, A.B., Elphic, R.C., Gasnault, O.M., Maurice, S., Moore, K.R., 2002. Library least squares analysis of Lunar Prospector gamma-ray spectra. *Lunar Planet. Sci. XXXIII*, 2012. Abstract.
- Rajmon, D., Spudis, P., 2004. Distribution and stratigraphy of basaltic units in maria Tranquilitatis and Fecunditatis: A Clementine perspective. *Meteor. Planet. Sci.* 39, 1699–1720.
- Reid, A., Jakes, P., 1974. Luna 16 revisited: The case for aluminous mare basalts. *Lunar Sci.* 13 (2), 627–629. Abstract.
- Reid, A., Taylor, G.J., Marvin, U.B.A.W.J., 1972. Luna 16: Relative proportions and petrologic significance of particles in the soil from Mare Fecunditatis. *Earth Planet. Sci. Lett.* 13, 286–298.
- Ridley, W.I., 1975. On high-alumina mare basalts. *Proc. Lunar Sci. Conf.* 6, 131–145.
- Schultz, P.H., Spudis, P.D., 1979. Evidence for ancient mare volcanism. *Proc. Lunar Sci. Conf.* 10, 2899–2918.
- Shearer, C.K., Papike, J.J., 1999. Magmatic evolution of the Moon. *Am. Mineral.* 84, 1469–1494.
- Shervais, J.W., Taylor, L.A., Lindstrom, M.M., 1985. Apollo 14 mare basalts: Petrology and geochemistry of clasts from consortium breccia 14321. *J. Geophys. Res.* 90, C375–C395.
- Shih, C.Y., Nyquist, L.E., 1989a. Isotopic and chemical constraints on models of aluminous mare basalts genesis. *Lunar Planet. Sci. XX*, 1002–1003. Abstract.
- Shih, C.Y., Nyquist, L.E., 1989b. Isotopic constraints on the petrogenesis of Apollo 14 igneous rocks. In: Taylor, G.J., Warren, P.H. (Eds.), *Workshop on Moon in Transition: Apollo 14, KREEP, and Evolved Lunar Rocks*, vol. 89–03. Lunar Planet. Inst., Houston, TX, pp. 128–136.
- Snyder, G.A., Taylor, L.A., Neal, C.R., 1992. A chemical model for generating the sources of mare basalts: Combined equilibrium and fractional crystallization of the lunar magmasphere. *Geochim. Cosmochim. Acta* 56, 3809–3823.
- Snyder, G.A., Borg, L.E., Nyquist, L.E., Taylor, L.A., 2000. Chronology and isotopic constraints on lunar evolution. In: Canup, R.M., Righter, K. (Eds.), *Origin of Earth and Moon*. Lunar Planet. Inst., Houston, pp. 361–395.
- Staid, M.I., Pieters, C.M., 2000. Integrated spectral analysis of mare soils and craters: Application to eastern nearside basalts. *Icarus* 145, 122–139.
- Strasheim, A., Jackson, P.F.S., Coetzee, J.H.J., Streloew, F.W.E., Wybenga, F.T., Gricius, A.J., Kokot, M.L., Scott, R.H., 1972. Analysis of lunar samples 14163, 14259, and 14321 with isotopic data for $^{7}\text{Li}/^{6}\text{Li}$. *Geochim. Cosmochim. Acta* 2, 1337–1342.
- Taylor, G.J., Warren, P., Ryder, G., Delano, J., Pieters, C., Lofgren, G., 1991. Lunar rocks. In: Heiken, G.H., Vaniman, D.T., French, B.M. (Eds.), *Lunar Sourcebook*. Cambridge Univ. Press, New York, pp. 183–284.
- Taylor, L.A., Shervais, J.W., Hunter, R.B., Shih, C.Y., Bansal, B.M., Wooden, J., Nyquist, L.E., Laul, L.C., 1983. Pre-4.2 AE mare basalt volcanism in the lunar highlands. *Earth Planet. Sci. Lett.* 66, 33–47.
- Taylor, S.R., Jakes, P., 1974. The geochemical evolution of the Moon. *Proc. Lunar Sci. Conf.* 5, 1287–1305.
- Taylor, S.R., Kaye, M., Muir, P., Nance, W., Rudowski, R., Ware, N., 1972. Composition of the lunar uplands: Chemistry of Apollo 14 samples from Fra Mauro. *Proc. Lunar Sci. Conf.* 3, 1231–1249.
- Vinogradov, A.P., 1971. Preliminary data on lunar ground brought to Earth by automatic probe "Luna-16". *Proc. Lunar Sci. Conf.* 2, 1–16.
- Warren, P.H., Kalleymen, G.W., Kyte, F.T., 1997. Siderophile element evidence indicates that Apollo 14 high-Al mare basalts are not impact melts. *Lunar Planet. Sci. XXVIII*, 1501–1502. Abstract.
- Wilcox, B.B., Lucey, P.G., Gillis, J.J., 2005. Mapping iron in the lunar mare: An improved approach. *J. Geophys. Res.* 110 (E11), doi:10.1029/2005JE002512.
- Wilhelms, D., 1987. The Geologic History of the Moon. U.S. Geological Survey Professional Paper 1348. U.S. Geological Survey, Washington, DC.
- Zeigler, R.A., Korotev, R.L., Haskin, L.A., Jolliff, B.L., Gillis, J.J., 2006. Petrography and geochemistry of five new Apollo 16 mare basalts and evidence for post-basin deposition of basaltic material at the site. *Meteor. Planet. Sci.* 41 (2), 263–284.